DOKUZ EYLÜL UNIVERSITY
GRADUATE SCHOOL OF NATURAL AND APPLIED SCIENCES

PRODUCTION AND APPLICATION OF ELECTROACTIVE POLYMERS BY USING PIEZOELECTRIC NANOMATERIALS

by
Bahar Şölen AKDEMİR

January, 2019
İZMİR

PRODUCTION AND APPLICATION OF ELECTROACTIVE POLYMERS BY USING PIEZOELECTRIC NANOMATERIALS

A Thesis Submitted to the
Graduate School of Natural and Applied Sciences of Dokuz Eylül University
In Partial Fulfillment of the Requirements for the Degree of Master of Science
in Nanoscience and Nanoengineering Program

by

Bahar Şölen AKDEMİR

January, 2019
İZMİR

M.Sc THESIS EXAMINATION RESULT FORM

We have read the thesis entitled **"PRODUCTION AND APPLICATION OF ELECTROACTIVE POLYMERS BY USING PIEZOELECTRIC NANOMATERIALS"** completed by **BAHAR ŞÖLEN AKDEMİR** under supervision of **ASSOC. PROF. DR. İHSAN MURAT KUŞOĞLU** and we certify that in our opinion it is fully adequate, in scope and in quality, as a thesis for the degree of Master of Science.

Assoc. Prof. Dr. İ. Murat KUŞOĞLU

Supervisor

Assoc. Prof. Dr. Uğur Gaudar

(Jury Member)

Assoc. Prof. Dr. M. Faruk Ebeoğlu

(Jury Member)

Prof.Dr. Kadriye ERTEKİN

Director
Graduate School of Natural and Applied Sciences

ACKNOWLEDGEMENT

I would first like to thank my thesis advisor Assoc. Prof. Dr. İ. Murat KUŞOĞLU. He allowed this paper to be my own work, but steered me with his advices and wide experiences.

I would also like to thank for their endless support who were involved in validation survey for this research project: the experts in Dokuz Eylül University Electronic Materials Production and Application Center (DEU-EMUM) to support me for characterization processes, the instructors and research assistants in Manisa Celal Bayar University for their advices and to support me for production processes.

Finally, I must express my very profound gratitude to my parents for providing me with unfailing support and continuous encouragement through the process of researching and writing this thesis. This accomplishment would not have been possible without them. Thank you.

This thesis was supported by the Scientific Research Project Unit of Dokuz Eylül University through the project number 2018.KB.FEN.025.

B. Şölen AKDEMİR

PRODUCTION AND APPLICATION OF ELECTROACTIVE POLYMER BY USING PIEZOELECTRIC NANOMATERIALS

ABSTRACT

In this research by using barium titanate and carbon nanotube additives composites having silicone elastomer (PDMS) matrix were made to produce electroactive polymer composite. First different temperatures and durations were examined to cure the PDMS silicon elastomer to obtain the one which has higher dielectric constant. After that to measure the barium titanate particle size, appropriate dispersant and particle amount optimization was made. Different weight percent amounts of barium titanate powder were mixed with the PDMS to determine optimum dielectric constant by LCR meter. CNT layer was coated onto the PDMS by stamping. Its morphological and electrical properties were observed by digital microscope. SEM, FTIR and DTA measurement were made to compare the surface morphology and particle distribution, bonding property change by effect of additives and curing regime respectively.

Keywords: Electroactive polymer, barium titanate, carbon nanotube, PDMS

PİEZOELEKTRİK NANOMALZEMELER KULLANILARAK ELEKTROAKTİF POLİMER ÜRETİMİ VE UYGULAMALARI

ÖZ

Bu çalışmada barium titanat ve karbon nanotüp katkıları kullanılarak silicon elastomer (PDMS) matrisli elektroaktif polimer kompozit üretilmiştir. Daha yüksek dielektrik katsayıya sahip PDMS silikon elastomeri bulabilmek için farklı kürleme sıcaklıkları ve süreleri denenmiştir. Daha sonra baryum titanantın tane boyut ölçümü için optimum dağıtıcı ve toz miktarlarının optimizasyon çalışması yapılmıştır. LCR metre kullanılarak ölçülen optimum dielektrik katsayıya sahip kompositi üretebilmek için ağırlıkça yüzde olarak farklı miktarlarda baryum titanat PDMS ile karıştırılmıştır. Karbon nanotüp tabakası damgalama yöntemiyle PDMS yüzeyine kaplanmıştır. Karbon nanotüp tabakasının yüzey ve elektriksel özellikleri dijital mikroskop kullanılarak incelenmiştir. Yüzey özelliklerini ve tane dağılımlarını gözlemleyebilmek için SEM, yapılan katkıların bağ özelliklerine etkisini incelemek için FTIR ve kürleme parametrelerini belirleyebilmek için de DTA analizleri yapılmıştır.

Anahtar Kelimeler: Elektroaktif polimer, baryum titanat, karbon nanotüp, PDMS

CONTENT

Page

LIST OF FIGURES

Page

LIST OF TABLES

Page

CHAPTER ONE
INTRODUCTION

Technology has been developing in recent years due to changing our daily life requirements quite rapidly. Because the new state-of-art technological areas came up like smart televisions, phones, cars, and high performance computers etc. To adapt these new technologies to our daily life, we need energy sources to fulfill the requirements of these kinds of technologies. Therefore new kinds of actuators are developed by using high technology materials like piezoelectric ceramics and electroactive polymers which are called smart materials.

Actuators provide energy to the systems by converting a form of energy to another one. Conventional actuators like electromotors and combustion engines (Madden et al., 2003) could not provide the energy needed for the state-of-art technological devices. Because these devices require smaller, lighter and more effective actuators. To overcome this issue new kind of actuators are developed by combining smart materials with actuator systems.

Smart materials are one of the candidate materials for these kinds of actuators. They are defined as materials which respond external stimulus in real time or near real time (Ribeiro, 2012; Shankar, Ghosh, & Spontak, 2007). They change one or more of their physical properties according to this visible and measurable external energy. This response should be repeatable, reversible, fast and significant (Shankar, Ghosh, & Spontak, 2009). Piezoelectric & electrostrictive ceramics, electroactive polymers, magnetostrictive materials, shape-memory materials and magnetorheological fluids are common examples of smart materials (Finkenstadt & Willett, 2005). In this dissertation piezoelectric ceramics and electroactive polymers are explained in detail.

Smart materials find a new application areas in every day. Technological improvement let us to use smart materials in different ways. The smart ski shown in figure 1.1 produced by Active Control eXperts, Cambridge, Massachusetts contains three different ceramic layer in a polymer part. It creates electrical energy by

movement of the skier (Richerson & Lee, 2018). Some ceramics are transparent to the electromagnetic waves despite opaque to visible light. This distinguishing property of ceramics compared with the metals opens a new application area of ceramics as smart materials in missiles. Additionally because of the extreme hardness they are used in body and vehicle armors to withstand the fast and energetic stresses.

Figure 1.1 Smart ski produced by Active Control eXperts, Cambridge, Massachusetts (Richerson & Lee, 2018)

At the beginning of the 1990s new class of polymer was emerged which responds to electric field by changing its size or shape. This class of polymers were named as "electroactive polymers". Actually the first electroactive response was derived by Rontgen in 1880 by using a natural rubber (Roentgen, 1880). In 1925, an electret which is a piezoelectric polymer was discovered by Eguchi (Eguchi, 1925). The following years by the discovery of PVDF (poly(vinylidenefluoride)) piezoelectric response, the researches about electroactive polymers get attention incrementally (Bar-Cohen, 2004).

Preliminarily their shape changes, strains were small. As the researches increase, the strain of electroactive polymers was developed as high as two orders of magnitude. Because of their similar response to the human muscles, they were named also as "artificial muscles". Scientists and engineers started to develop biomimetic robotics. In 2002, a first commercial electroactive material was produced by a Japan company named as Eamex. It was a robotic fish swimming in water by using an inductive coil instead of battery as shown in figure 1.2 (Bar-Cohen, 2004). Detail informations about the EAPs were given in later.

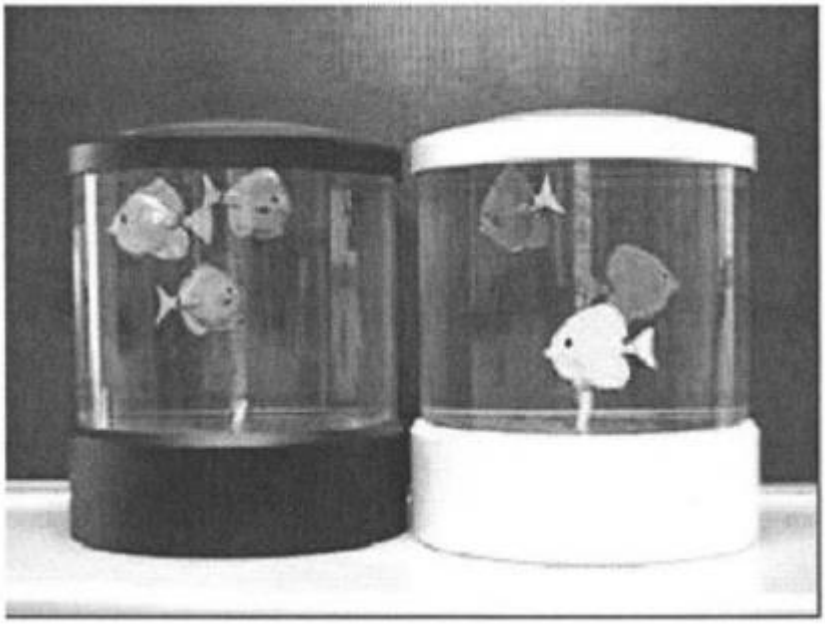

Figure 1.2 First commercial EAP robotic fish (Bar-Cohen, 2004)

The scope of this thesis the PDMS composite was examined containing different amounts of $BaTiO_3$ nanoparticles. Experimental studies were pursued to obtain the effect of $BaTiO_3$ nanoparticle additives on the dielectric constant of the PDMS affecting the electroactive response.

In the scope of this dissertation, brief information about ceramics and detail information about piezoelectric ceramics will be given in chapter two. In chapter three, after mentioning general properties of polymers, detail information will be given about electroactive polymers. Finally materials and the characterization methods which are used in this thesis will be given in chapter four together with the experimental procedure.

CHAPTER TWO
POLYMERS: ELECTROACTIVE POLYMERS

2.1 Polymers

Polymer comes from Greek word (poly means “many”, meres means “part”). It is formed from many small units coming together to form long polymer chains which are called monomers. Monomers are the smallest unit of the polymer. In the figure 2.1 polyethylene monomer unit is given as an example with the unstable end points (Beşergil, 2003; McCrum, Buckley, & Bucknall, 1997; Saçak, 2012).

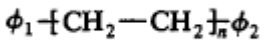

Figure 2.1 Example of polyethylene monomer (McCrum et al., 1997)

There are two type of reaction that monomers come together: addition reaction and condensation reaction. This is called polymerization. In addition polymerization there are two unstable ends on the monomer unit. During the polymerization reaction the double bond at these unstable end points opens and other monomer unit attaches to this end. The creating free electron by opening the double bond forms a bond with other monomer and creates long chains. The other polymerization reaction is the condensation reaction. The creations of polymer chain in this type of polymerization in step by step and all reactions have their own unstable ends. Some polymers contain more than one monomer units and they are called copolymers. By adjusting these ratios of monomers, the different types of polymers having specific properties could be produced. This process is similar to alloying in metals which includes solid solution process (Beşergil, 2003; McCrum et al., 1997; Saçak, 2012).

Polymers could have different type of chain structure like linear or side-branched. In figure 2.2 an example of linear and side-branched polymer is given. Due to this structural difference their mechanical properties differ from each other like elastic modulus, melting temperature and toughness (Beşergil, 2003; McCrum et al., 1997; Saçak, 2012).

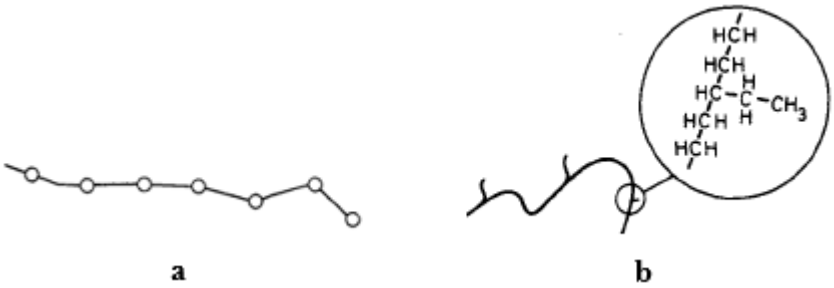

Figure 2.2 a. linear chain structure b. side-branched chain structure (McCrum et al., 1997)

Depending on the bonding type some polymers could be polymerized and melted again and again to re-use them. These types of polymers are called thermoplastics. They can be recycled. However some polymers contain chemical bonds to keep polymer chains together called cross-links. In figure 2.3 a crosslinked polymer structure is given. The dark points inside of the squares are the crosslinking points holding the chains together. These cross-linked polymers could not be re-cycled. These cross-links only may decompose by chemical reactions like burning. They are called thermosets (Beşergil, 2003; McCrum et al., 1997; Saçak, 2012).

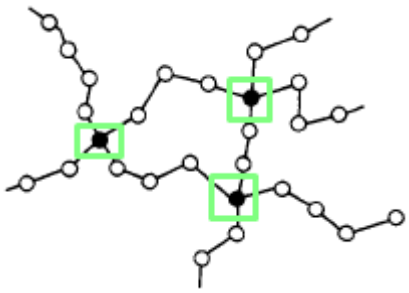

Figure 2.3 Cross-linked polymer structure (McCrum et al., 1997)

2.2 Electroactive Polymers (EAP)

EAPs exhibit considerable stress and/or strain upon electrical stimulation with a change in shape or size (Bar-Cohen, 2005; Finkenstadt & Willett, 2005; Kornbluh et al., 1999; Pelrine, Kornbluh, Pei, & Joseph, 2000; Ren, 2007; Ribeiro, 2012; Shankar et al., 2007, 2009). They create a motion as actuators like torque generation in conventional electric motors (Shankar et al., 2007). However, they are smaller, lighter and more effective than conventional actuators (Madden et al., 2003). EAPs convert electrical energy to a mechanical energy (Cheng et al., 2001; Pelrine et al., 2000; Shankar et al., 2007, 2009). They are smart materials which respond their environmental changes like temperature, pH, light, magnetic and electric field in a controllable way (Bar-Cohen, 2005; Finkenstadt & Willett, 2005; Kornbluh et al., 1999; Pelrine et al., 2000; Ren, 2007; Ribeiro, 2012; Shankar et al., 2007, 2009). They are also considered as high performance actuators (Bar-Cohen, 2005; Kornbluh et al., 1999; Pelrine et al., 2000; Ren, 2007).

Generally EAPs are used in high technology required applications like implants in biomedical, artificial muscles, nano-related biomimetic actuators etc. (Bar-Cohen, 2005; Finkenstadt & Willett, 2005; Pelrine et al., 2000; Ribeiro, 2012; Shankar et al., 2007, 2009). In addition to these applications, in electronic sector EAPs are mostly preferable as mini- and micro-robotic components, visual displays, flat panel speakers, acoustic transducers for underwater applications etc. (Cheng et al., 2001; Pelrine et al., 2000; Shankar et al., 2007).

EAPs are favored in high technology applications due to their various advantages like good electromechanical properties, large actuation strain, comparatively low actuation stress (Shankar et al., 2009), easily processable, light weight, low cost (Cheng et al., 2001; Kornbluh et al., 1999; Shankar et al., 2007, 2009), flexible behavior and high efficiency at small scales (Shankar et al., 2007). Also EAPs have actuation strains as high as two orders of magnitude than EACs. By comparison with SMAs, EAPs exhibit higher response speed, cycle time and lower density (Bar-Cohen, 2005; Shankar et al., 2009). On the other hand insufficient response speed (Pelrine et

al., 2000) and low electromechanical conversion efficiency (Cheng et al., 2001) limits their applications.

EAPs basically divided into two main group as electronic EAP and ionic EAP. In the figure 2.4 there are sub-groups of these two main EAPs. In the scope of this thesis; only conductive polymers, ferroelectric polymers and dielectric elastomers are described briefly (Bar-Cohen, Kim, Choi, & Madden, 2007; Ozsecen, 2010; Ribeiro, 2012).

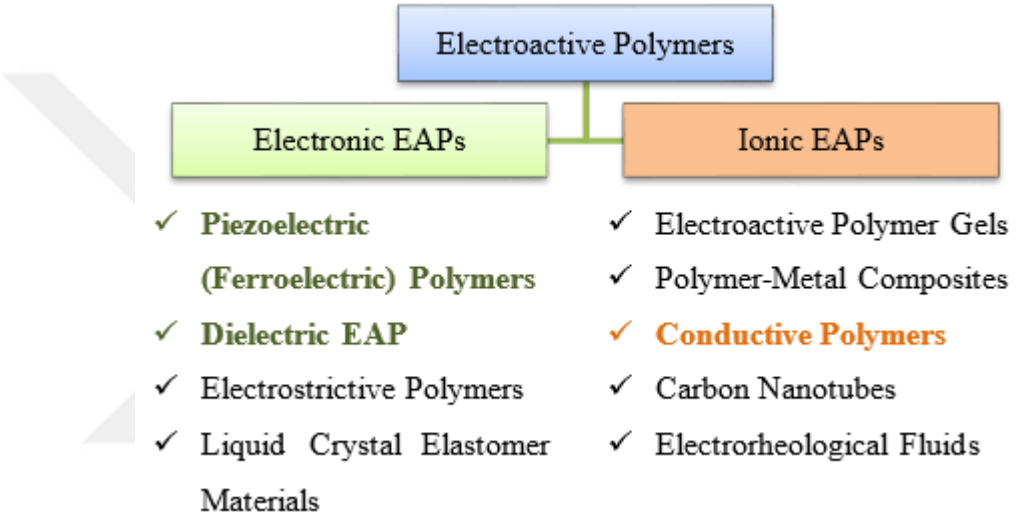

Figure 2.4 Scheme of the main EAP types (Ozsecen, 2010)

2.2.1 Conductive Polymers

Conductive polymers are based on organic polymers and an electrolyte layer or film. The actuators made of these kinds of polymers could be bilayer or trilayer. In figure 2.5 a schematic representation of a trilayer actuator is shown.

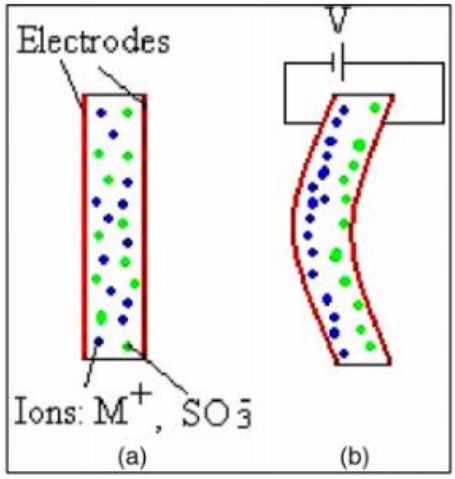

Figure 2.5 Trilayer conductive polymer actuator (Godfrey, 2017)

The mechanism is based on the mainly positive charged ion diffusion. During electrical activation, two different type of reaction occurs, one is oxidation and the other one is reduction. Positively charged ions start to move to the cathode layer. The cathode layer shrinks due to the reduction reaction. Oppositely, oxidation reaction takes place in the anode layer and the anode layer expands. Due to this chemical reactions trilayer actuator bends in one direction. To bend the actuator through the opposite direction, it is enough to apply opposite voltage (Godfrey, 2017; Lai, 2015).

2.2.2 Ferroelectric Polymers

Ferroelectric polymers behave like piezoelectric material which is explained later. They convert electrical energy to mechanical energy and mechanical energy to the electrical one which is called direct and indirect effect respectively. They have permanent dipoles whether electrical field exists or not. These dipoles are reoriented depending on the electrical field direction. Ferroelectric materials could be used in different environments in the temperature range between 20-80°C like air, water or even in vacuum (Godfrey, 2017; Lai, 2015). General response mechanism of the ferroelectric materials is given in the figure 2.6.

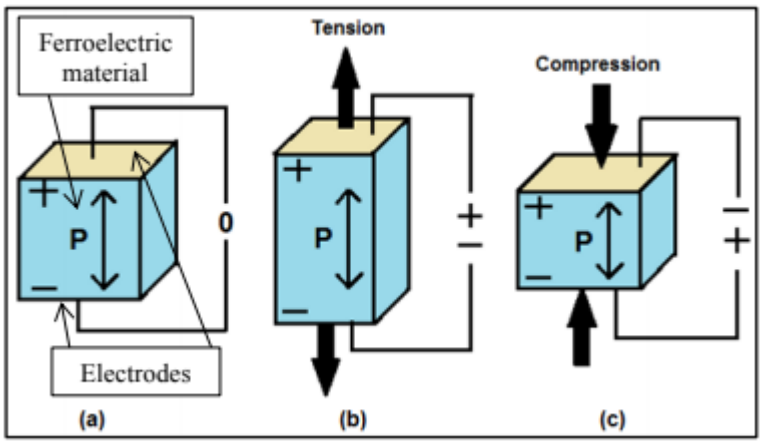

Figure 2.6 Ferroelectric polymer working mechanism (Godfrey, 2017)

Like non-centrosymmetric piezoelectric materials, non-conducting and dielectric polymers exhibit ferroelectricity by changing permanent dipole orientation with electric field. This dipole orientation causes the polymer length is increased due to stretching which is called as electrostriction. In the figure 2.7, PVDF (poly (vinylidenefluoride)) which is the most common ferroelectric polymer, orientation and stretch is shown to cause ferroelectricity (Cakmak, 2014).

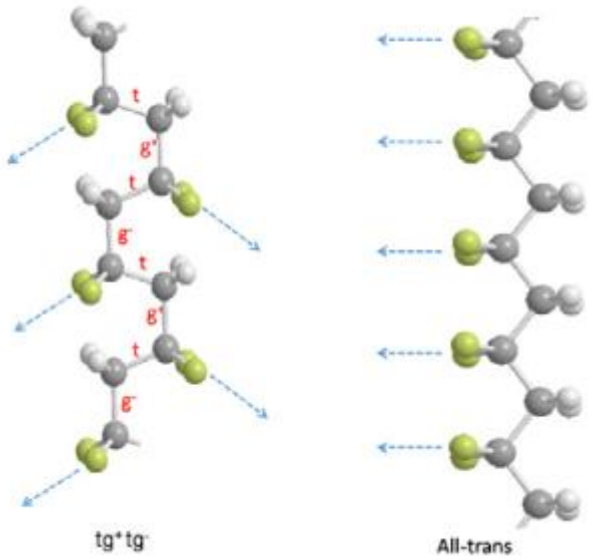

Figure 2.7 Ferroelectricity in PVDF (Cakmak, 2014)

2.2.3 Dielectric Elastomers

Dielectric elastomer is based on a dielectric polymer and two electrode which have contact with the polymer shown in figure 2.8. When voltage is applied dielectric elastomer will expand. Therefore the dielectric elastomer should have high dielectric constant and deformation capability. Due to the repelling of accumulated opposite charges on different surfaces; electrodes squeeze the elastomer and make it shrinks in thickness also expands in planar surface. Generally this effect is called “Maxwell stress” caused by the coulombic forces (Godfrey, 2017; W. Hu, 2015; Lai, 2015; Niu, 2013).

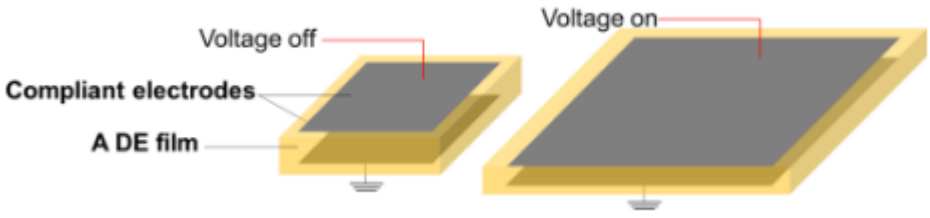

Figure 2.8 Dielectric elastomer response against the applied voltage (Hu, 2015)

Dielectric elastomers have a lot of advantages against other type of materials like low density, high deformability, high strain and high energy density. It is the most preferable material to mimic the nature, because it has the most similar properties with the mammalian muscles. The relation is shown in the table 2.1 (Hu, 2015).

Table 2.1 Property relations between different electroactive materials (Hu, 2015)

Property	Density (g/cm^3)	Modulus (MPa)	Strain (%)	Energy density (kJ/m^3)
Mammalian Muscle	1	10-60	20-40	8-40
SMA (shape memory alloys)	6	20k-80k	1-8	>1k
Piezoelectric ceramic	8	70k	0.2	100
Conductive polymer	1.2	500	2-12	70-100
Ferroelectric polymer	2	400-1200	3-10	1k
Dielectric elastomer	1	0.1-3	~100	1k

*k=1000

2.3 Polydimethylsiloxane (PDMS)

Polydimethylsiloxane has excellent thermal, mechanical and elastic properties. Additionally it has good environmental and chemical stability. The composites consisting PDMS as a polymer have large temperature range usage (Chen, Lu, Wu, & Chen, 2007; Nayak, Chaki, & Khastgir, 2014). Additionally PDMS is biocompatible and could be used in biomaterial applications (Mata, Fleischman, & Roy, 2005). Due to its optical transparency it is used in elastic microchips to replicate the circuits (S. W. Lee & Lee, 2008). Thermal stability, chemically inertness, easy production properties with the previously mentioned ones make PDMS highly preferable for different kind of applications like aerospace, automobile and textile industries (Martinček, Turek, & Tarjányi, 2014). Its properties and related application relationships are given in the table 2.2.

Table 2.2 Different properties of PDMS and their applications (McDonald & Whitesides, 2002)

Property	Characteristic	Application
Optical	Transparent; UV cutoff, 240 nm	Optical detection from 240 to 1100 nm
Electrical	Insulating; breakdown voltage, $2x10^7$ V/m	Allows embedded circuits; intentional breakdown to open connections
Mechanical	Elastomeric; tunable Young's modulus, typical value of ~750 kPa	Conforms to surfaces; allows actuation by reversible deformation; facilitates release from molds
Thermal	Insulating; thermal conductivity, 0.2 W/(m·K); coefficient of thermal expansion, 310 μm/(m·°C)	Can be used to insulate heated solutions; does not allow dissipation of resistive heating from electrophoretic separation
Interfacial	Low surface free energy ~20 erg/cm^2	Replicates release easily from molds; can be reversibly sealed to materials
Permeability	Impermeable to liquid water; permeable to gases and nonpolar organic solvents	Contains aqueous solutions in channels; allow gas transport through the bulk material; incompatible with many organic solvents
Reactivity	Inert; can be oxidized by exposure to a plasma; $Bu_4N^+F^-$ ((TBA)F)	Unreactive toward most reagents; surface can be etched; can be modified to be hydrophilic and also reactive toward silanes; etching with (TBA)F can alter topography of surfaces
Toxicity	nontoxic	Can be implanted in vivo; supports mammalian cell growth

PDMS is both inorganic and organic polymer. Because of the silicone backbone and the weak attraction bonds between them makes PDMS as an inorganic polymer. At the same time because of the organic networks between inorganic silicone backbones, it is called organic polymer. This duality gives PDMS excellent properties like thermal and chemical resistance coming from ceramics, elasticity and producibility from organic polymers (Andersson & Hjertberg, 2003; Eduok, Faye, & Szpunar, 2017). As a silicone backbone the repeating unit of PDMS which creates chemical structure is given in figure 2.9 (Yilgör, E. & Yilgör, I., 2014).

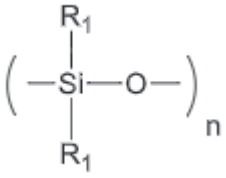

Figure 2.9 Repeating unit of PDMS (Yilgör, E. & Yilgör, I., 2014)

PDMS is generally purchased from commercial companies like Dow Corning Corporation and named as Sylgard 184. It contains two different parts; one is polymer base and the other one is the curing agent. To produce PDMS polymer, these two components should be mixed together as in ratio 10:1 (base:curing agent) (Andersson & Hjertberg, 2003; Bistričič, Borjanovič, Zamboni, Jakšič, & McGuire, 2014; Eduok et al., 2017).

Curing mechanism of the PDMS is based on the hydrosilation reaction process. The schematic representation of this process is given in figure 2.10. The first structure in the figure is crosslinker (poly-(dimethyl-methyl-hydrogensiloxane)) containing silyl group (SiH). The second one is polymer base (vinyl-terminated PDMS) containing vinyl group (-CH=CH_2). The curing reaction occurs between these two groups by creating ethylene bridges (-CH_2-CH_2) with the Pt catalyst coming from crosslinker (Andersson & Hjertberg, 2003; Bistričič et al., 2014; Eduok et al., 2017).

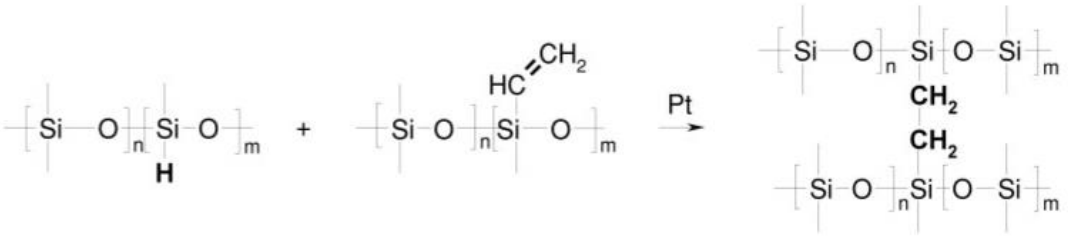

Figure 2.10 Curing reaction of the PDMS (Andersson & Hjertberg, 2003)

CHAPTER THREE
EAP BY USING PIEZOELECTRIC CERAMICS

3.1 Materials

As silicon elastomer PDMS (polydimethylsiloxane) is Sylgard 184 from DOWSIL contains two parts. One is polymer base and the other one is crosslinking agent. $BaTiO_3$ as piezoelectric ceramic nanoparticles was purchased from one of the Turkish company named as Nanografi at Ankara, Turkey. The product was made in Turkey. DTA, FTIR and XRD measurements were done on the as-received particles. All results were supported from the literature (Cho & Hamada, 1998; Groza & Surmeian, 2015; J. Lee et al., 2013; Malghe, Gurjar, & Dharwadkar, 2004; Moghtada & Ashiri, 2016). All other chemicals were purchased from local companies.

3.2 Experimental Procedure

3.2.1 Production Method

PDMS were mixed as a ratio 10:1 (polymer base:crosslinker) according to the technical data sheet. After manual mixing, it was poured into metal mold including 4 cavities having 20 mm length, 5 mm width and 500 μm thickness each. Then it was put into vacuum during 15 min under 700 mm Hg to remove the air bubbles coming from mixing. Finally it was cured at specified temperature and duration. The schematic representation of these steps were given at figure 3.1.

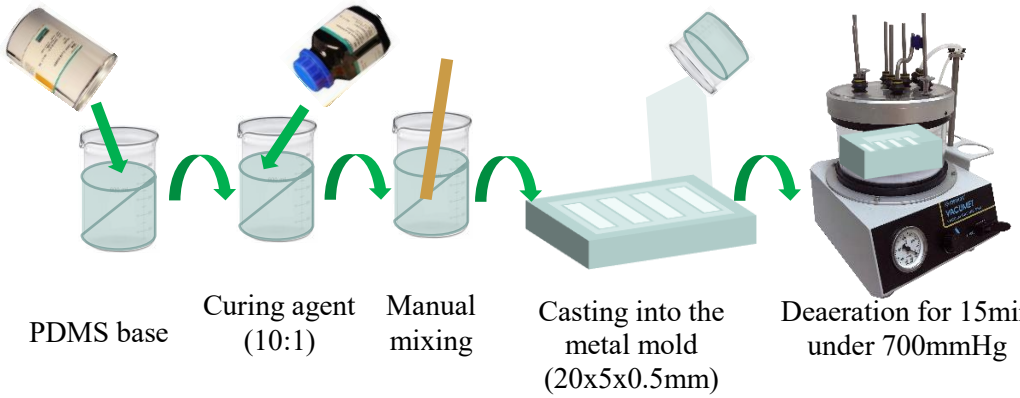

Figure 3.1 Production steps of PDMS silicone elastomer (Personal archive, 2018)

To prepare $BaTiO_3$ containing PDMS composite first $BaTiO_3$ particles were mixed with toluene to get homogeneous dispersion then added into the PDMS base. After that the mixture was put into the ultrasonic mixer during 60 min. After mixing, the curing agent was added and all the remaining process was the same. The schematic representation of this process is given in the figure 3.2.

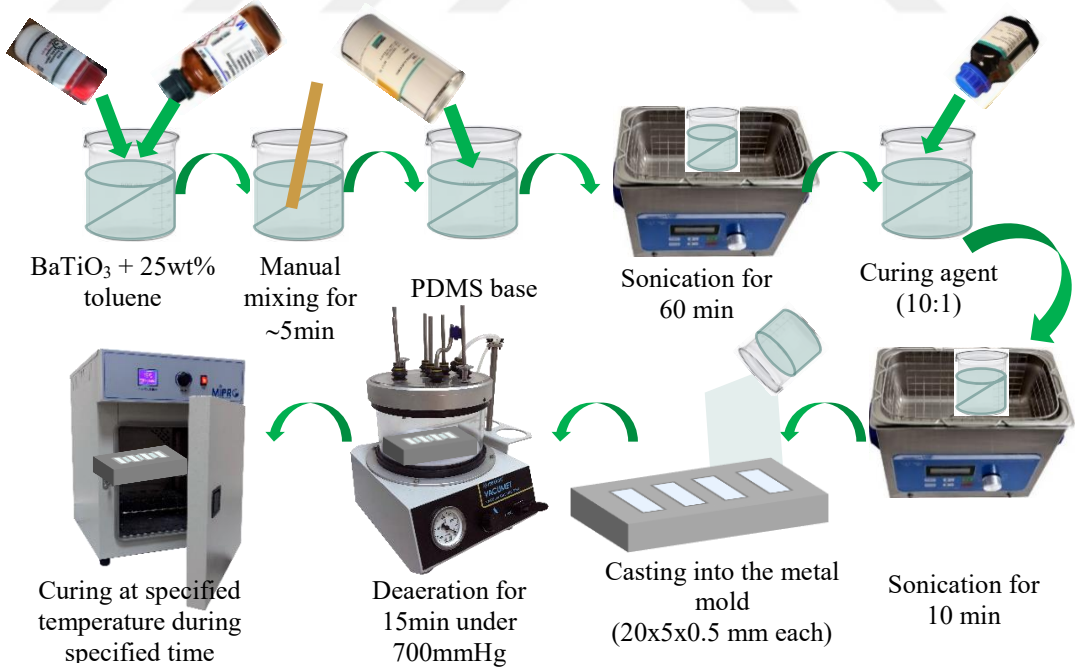

Figure 3.2 Production steps of BaTiO3 containing PDMS composite (Personal archive, 2018)

3.2.2 Characterization

Particle size measurement was made by using Malvern Nano ZS. For morphological examinations COXEM EM-30 Plus scanning electron microscopy was used. To get information about bonding type FTIR analyzes were examined by using Thermo Scientific NICOLET iS10. Thermogravimetric analyzes were made by Perkin Elmer STA 6000. ViTiny UM12 digital microscope was used to obtain high magnification optical images, videos and dimensional measurement. Dielectric constant calculations were made by using capacitance values obtaining by HIOKI LCR meter.

3.3 Results and Discussion

3.3.1 Particle Size Measurement

Particle size distribution (PSD) of nanoparticles are generally mixed into a deionized water in a certain amount to form a solution where the laser counts the particles in this medium (Sarıtaş, Türker, & Durlu, 2007). Nanoparticles tend to agglomerate in medium during laser PSD measurement. To overcome this problem, several surfactants are widely used in laser particle size distribution technique to avoid nanoparticles agglomeration during measurements. In this study, SHMP (sodium hexametaphosphate) was choosen as a surfactant. To achieve optimum distribution and particle size measurement, two steps optimization was made. In the first step, the $BaTiO_3$ content was kept constant and SHMP content was changed. After determining optimum SHMP content, secondly $BaTiO_3$ content was changed. The results were given at the figure 3.3. According to optimization studies of medium containing SHMP, $BaTiO_3$ and water, it is found that the solution having 1wt% SHMP and 0.5wt% $BaTiO_3$ nanoparticles reflects the optimum conditions for laser PSD measurement.

As shown in the graphs having 1wt% SHMP and 0.5wt% $BaTiO_3$, the average particle size of the $BaTiO_3$ nanoparticles is 192 nm. As committed, the $BaTiO_3$ particles are smaller than 300nm.

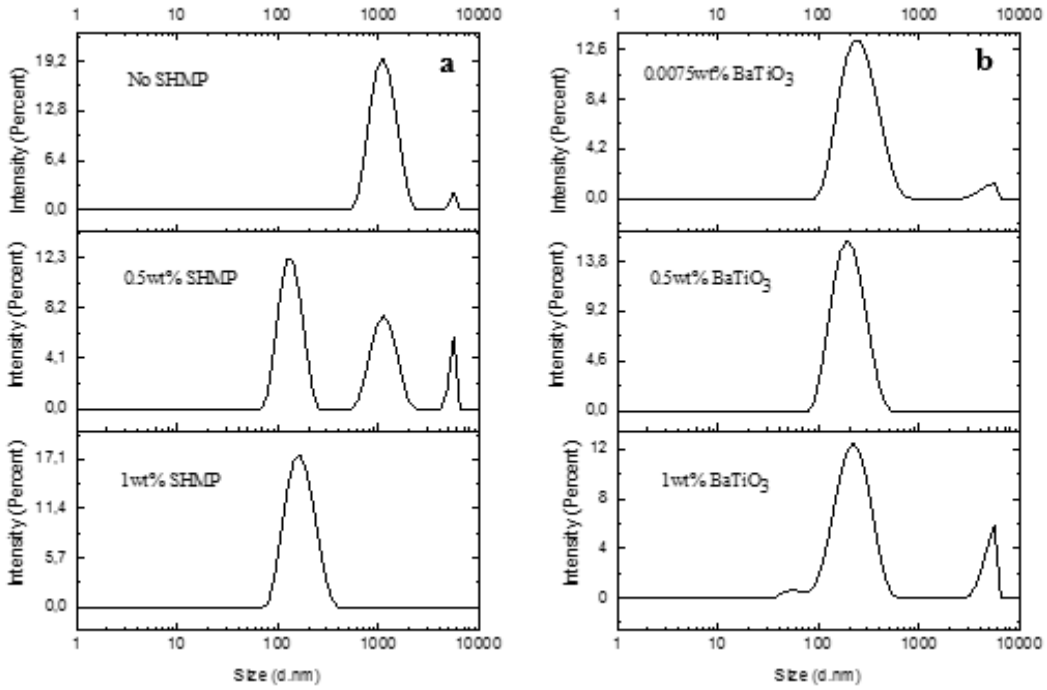

Figure 3.3 Particle size analyzes of $BaTiO_3$ powder a. optimization of dispersant amount b. optimization of powder amount

3.3.2 Dielectric Constant Measurement

To make a measurement optimization three different home-made experimental setup were constructed. All setups are given in figure 3.4. In setup-1, the sample was pressed directly between the clamps. In setup-2, the sample was placed between two wood plates. Then a weight was placed above the wood rods to sustain linear position and fixed pressure. In setup-3, again sample was placed between two wood rods. This time wood rods were pressed between the clamps. In all setups, aluminum tape was attached to the clamps as an electrode.

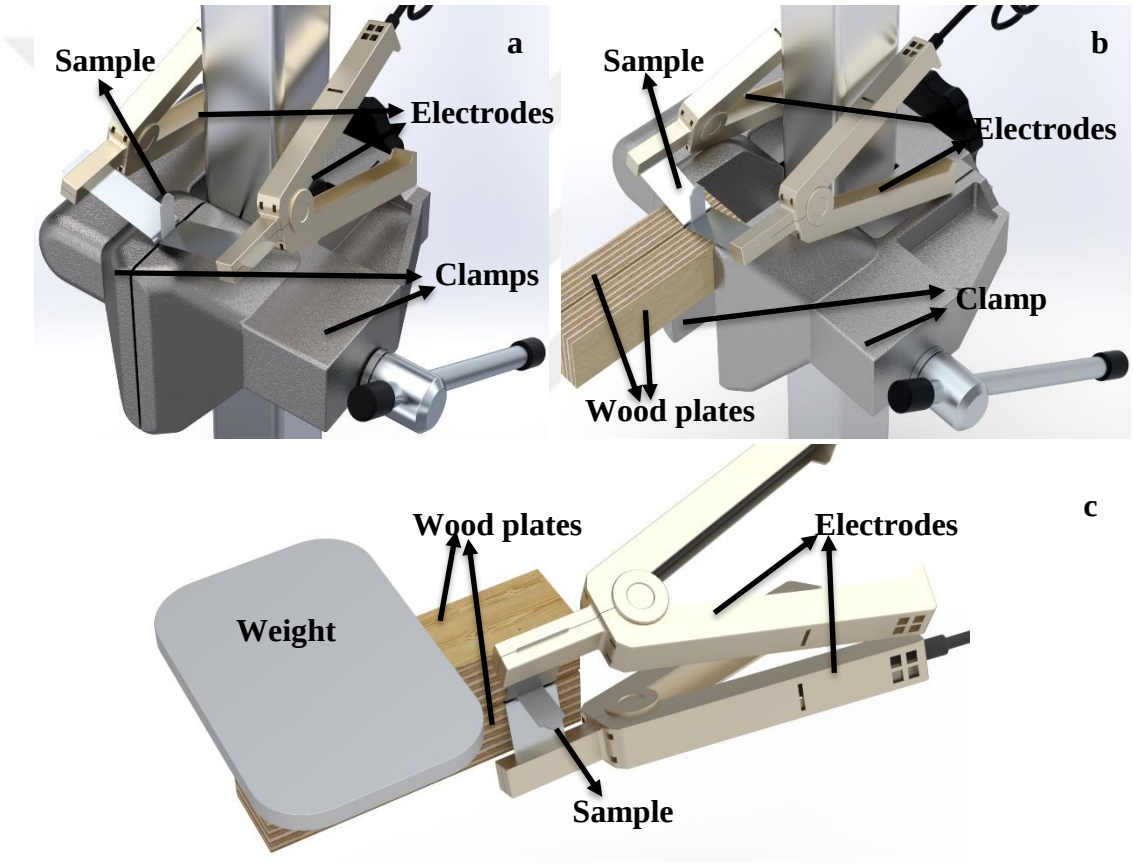

Figure 3.4 Dielectric constant measurement setups a. setup-1 b. setup-3 c. setup-2

The measured capacitance values are strongly depended on the pressure that applied to the sample. Because of the home-made setups, it was hard to sustain constant pressure during the experiment. Therefore it was found that the most reliable data were obtained with setup-2.

With LCR meter the capacitance values were measured between 100 Hz and 100 kHz. To compare the results the capacitance values at 10 kHz were chosen (Bai, Cheng, Bharti, Xu, & Zhang, 2000; W. Hu, 2015; Jiang et al., 2011; Ren, 2007; Xie, Zhu, Wei, Xu, & Xu, 2005).

3.3.3 The Effect of Curing Conditions on the Dielectric Constant of PDMS

To optimize the curing conditions of PDMS several temperatures ranging between 25-150°C and several durations from 10 min. to 24 hours (S. W. Lee & Lee, 2008; Madsen, Feidenhans'l, Hansen, Garnæs, & Dirscherl, 2014; Moraes, Sun, & Simmons, 2009; Schmid & Michel, 2000; Wu, Odom, Chiu, & Whitesides, 2003) obtaining from literature were examined (S. W. Lee & Lee, 2008; Moraes et al., 2009; Schmid & Michel, 2000). The given sample codes for curing conditions of PDMS were given at table 3.1.

Table 3.1 Curing conditions

Sample Code	Temperature (°C)	Time
P25/24	25	24 h
P40/4	40	4 h
P40/6	40	6 h
P60/3	60	3 h
P60/4	60	4 h
P80/1	80	1 h
P80/2	80	2 h
P80/3	80	3 h
P100/35	100*	35 min
P125/20	125*	20 min
P150/10	150*	10 min

* From technical data sheet of PDMS (Corning, 2013).

For the graphs, to make it easier "10035" abbreviation was used to describe curing of PDMS at 100°C for 35min. According to these, the dielectric constant values of various samples cured at different conditions are given in figure 3.5. The points are indicated as the average values of six capacitance measurement by LCR meter. Standard deviations are shown in graph as error bars. Their variations are because of

the pressure dependence nature of the process as mentioned previously in dielectric constant measurement optimization.

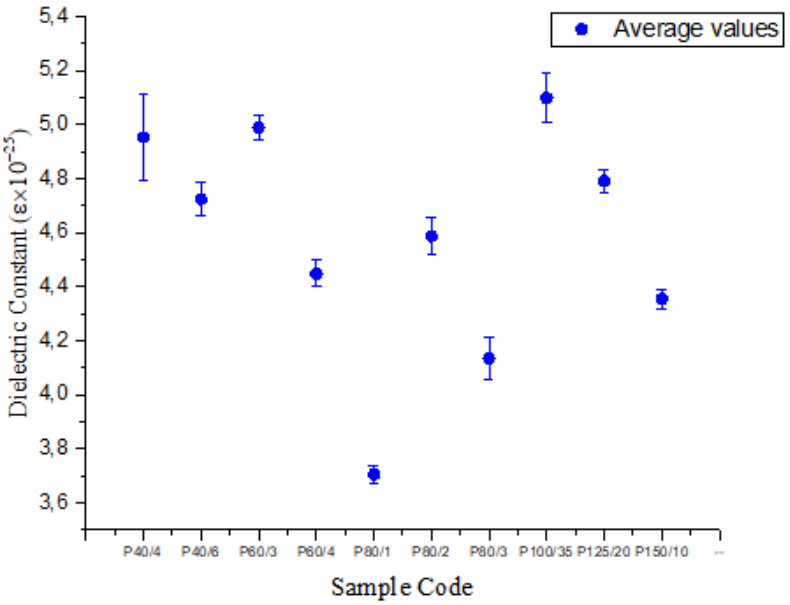

Figure 3.5 Dielectric constants of samples cured at different conditions

FTIR results of different curing parameters were analyzed as shown in figure 3.6. To compare FTIR data, only the samples which have the highest dielectric constant in each curing temperature were used. There is no significant effect of the curing temperature and duration to the bonding properties. The peaks describes transmittance values of different bonding types at specified wavenumber shown in figure 3.6. At 2962 cm^{-1} the peak belongs C-H stretching in CH_3. CH_3 symmetric and asymmetric bending in Si-CH_3 is related with the peak at 1445 cm^{-1}, 1412 cm^{-1} and 1257 cm^{-1}. The peak at around 1050 cm^{-1} is related with the Si-O-Si bonds. The peaks between 800 and 600 cm^{-1} are related with the CH_3 rocking in Si-CH absorption (Groza & Surmeian, 2015; J. Lee et al., 2013).

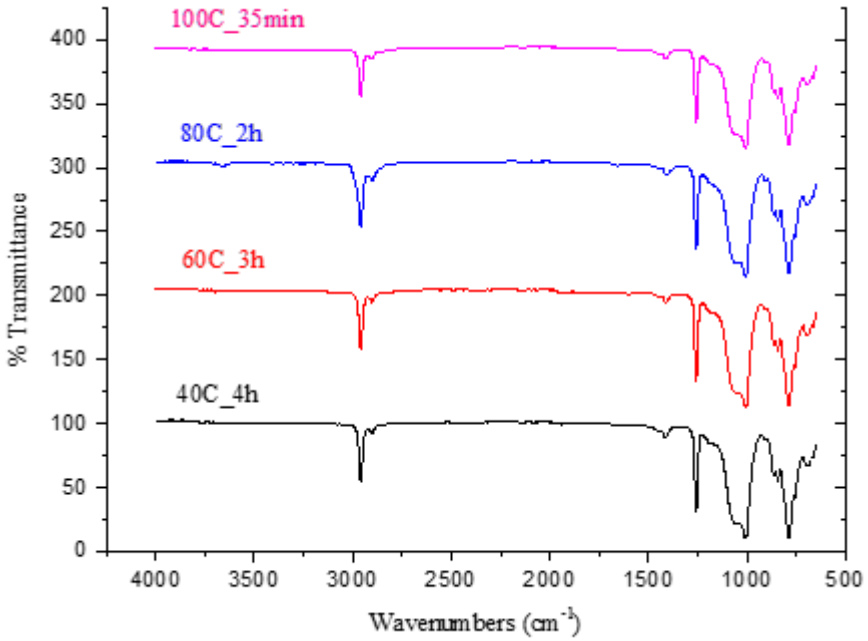

Figure 3.6 FTIR results of samples cured at different temperatures and times

After set-up optimization according to the dielectric constants, the sample which is cured at 100°C for 35 min. found to have the highest dielectric constant value. Because of that, the optimum curing condition was held as 100°C and 35 min. According to these results, SEM analyses were made to observe the surface morphology. The SEM images of samples which were cured at 40, 60, 80 and 100°C are shown in the figure 3.7. As shown in the figure sample surfaces were smooth. However for 80C_1h sample, a crack was observed on the surface shown in figure 3.8-a. The reason is that at 70°C there is an exothermic peak in DTA result related with the outgassing shown in figure 3.8-b. There were no observable cracks formation on 40C_4h, 60C_3h and 100C_35min samples.

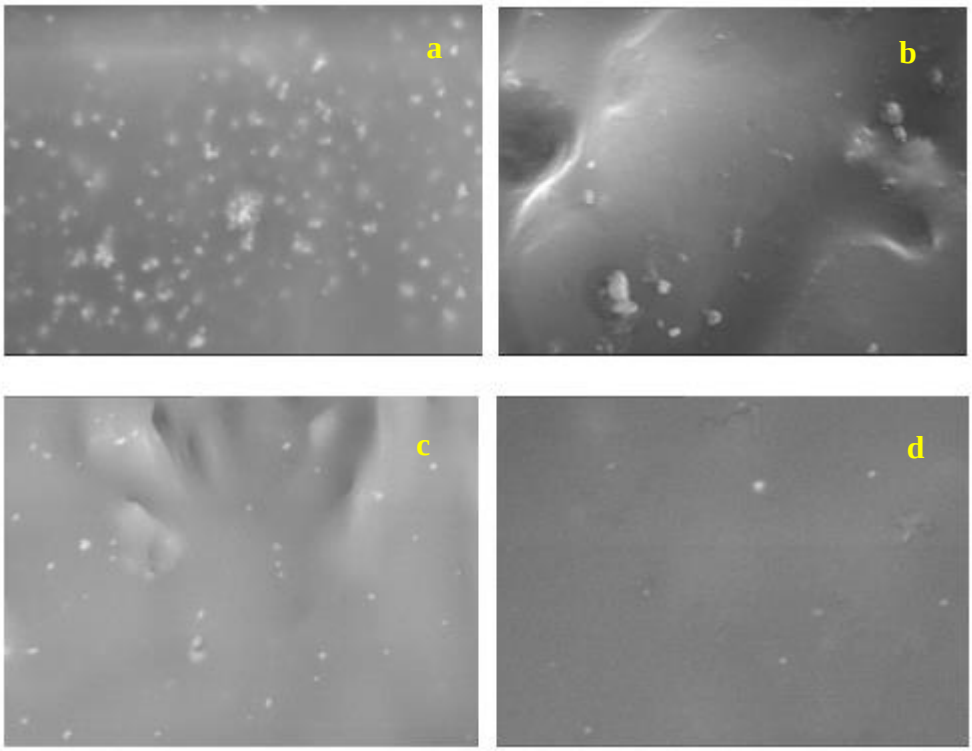

Figure 3.7 SEM images a. 40C_4h (x10k SEI) b. 60C_3h (x10k SEI) c. 80C_1h (x10k BEC), d. 100C_35min (x10k BEC)

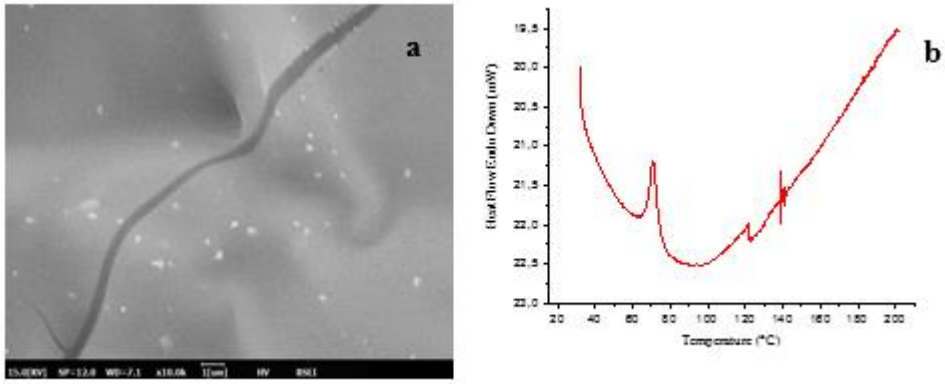

Figure 3.8 a. SEM image of 80C_1h sample b. DTA graph of 80C_1h sample

3.3.4 The Effect of $BaTiO_3$ Addition on the Dielectric Constant of PDMS Nanocomposites

To examine the $BaTiO_3$ addition effect on PDMS matrix, several ratios were prepared. The sample codes for several PDMS/$BaTiO_3$ compositions which are cured at 100°C for 35 min. are given in table 3.2. The ratios in front of the B refer to the wt. % $BaTiO_3$ mixed to PDMS. For example; 100C_35min_0.5B means that the sample contains 0.5 wt. % $BaTiO_3$ and cured at 100°C during 35 min.

Table 3.2 Sample codes of composites containing different amounts of $BaTiO_3$

Sample Code	**wt. % $BaTiO_3$**
P	0
P_0.5B	0.5
P_0.75B	0.75
P_1B	1
P_2.5B	2.5
P_5B	5
P_7.5B	7.5
P_10B	10
P_30B	30

The dielectric constant variation is given in figure 3.9. As shown in the graph, the dots represent the average dielectric constant values regarding composites containing different amounts of $BaTiO_3$ nanoparticles. There is an increase in dielectric constant until 1 wt. %. After this value there is a significant decrease with increasing $BaTiO_3$ content. According to the literature for nanomaterials there is a percolation threshold which is around 1 wt. %. After this percolation threshold for some reason properties begin to decrease (Chen et al., 2007). For our research this percolation threshold is obviously observable for dielectric constant.

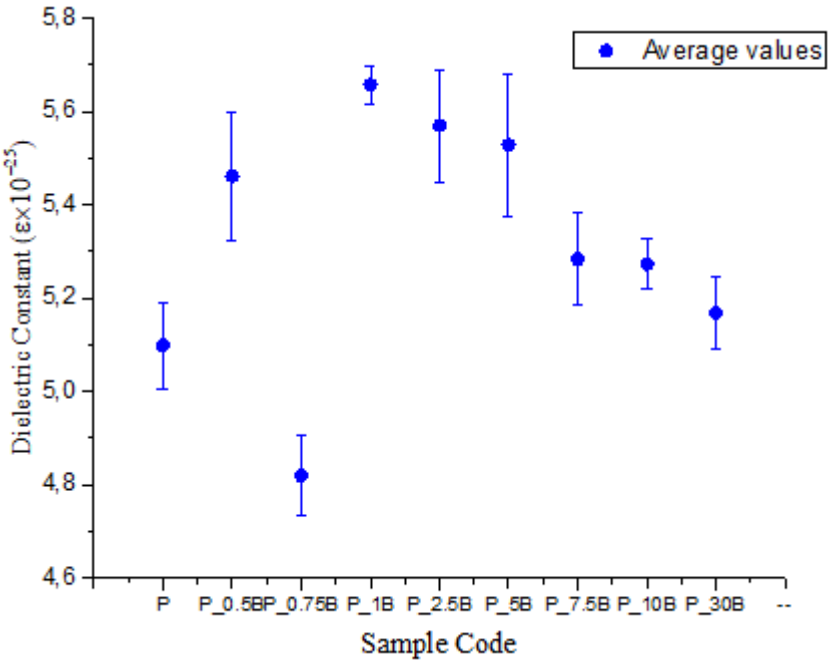

Figure 3.9 Dielectric constants of samples containing different amounts of $BaTiO_3$ additives

The $BaTiO_3$ particles in P-1B sample is shown in figure 3.10. Because of the very small amount of weight percentage, there are few particles on the image in high magnification (x 10k). On the contrary of the 100C_35min PDMS sample without $BaTiO_3$ filler, there are cracks on the surface. The reason is that by addition of $BaTiO_3$ particles into the PDMS matrix, the elasticity of the silicon rubber decreases (A. Bele, Cazacu, Stiubianu, & Vlad, 2014; Adrian Bele, Cazacu, Stiubianu, Vlad, & Ignat, 2015; Adrian Bele, Stiubianu, Varganici, Ignat, & Cazacu, 2015; Nayak, Chaki, & Khastgir, 2013).

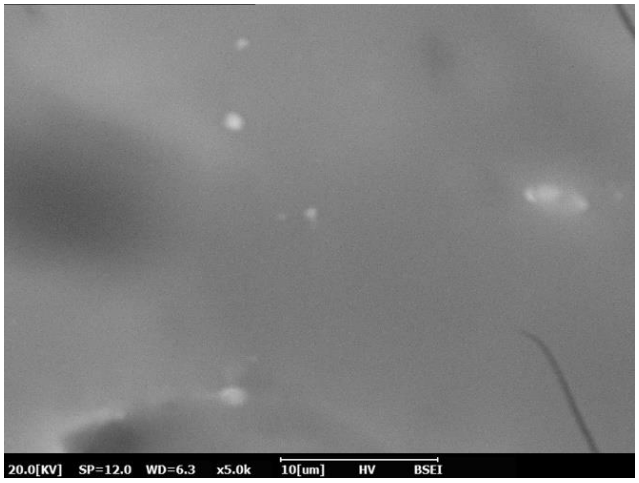

Figure 3.10 SEM image of the sample cured at 100C during 35 min. and containing 1 wt. % $BaTiO_3$

To examine the effect of $BaTiO_3$ in the PDMS on the bonding properties, FTIR analysis were made. The comparable FTIR data belonging to the $BaTiO_3$, 100C_35min and 100C_35min_10B samples were given in the figure 3.11. There is no observable effect of $BaTiO_3$ on the bonding properties because of the dominant peaks of PDMS. The peaks at around 3600 cm^{-1} which belongs to $BaTiO_3$ is related with the O-H bonds coming from moisture content at the surface of $BaTiO_3$ particles (Moghtada & Ashiri, 2016). In figure 3.12, to observe the effect of $BaTiO_3$ content 100C_35min, 100C_35min_10B and 100C_35min_30B samples were compared. As seen in the figure, at sample containing 10 wt. % $BaTiO_3$ the transmittance between 1500 and 1000 cm^{-1} wavelength was decreased.

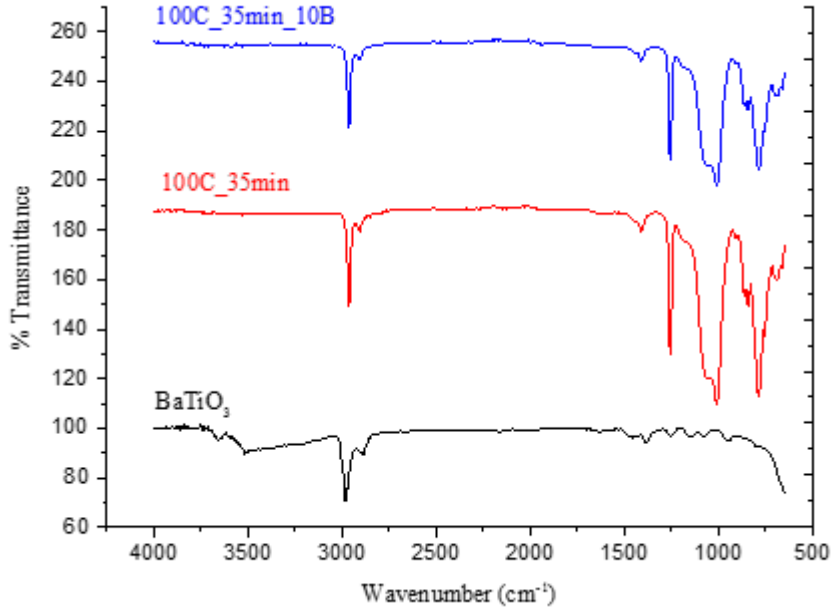

Figure 3.11 Comparable FTIR data graph to observe $BaTiO_3$ effect on the bond properties

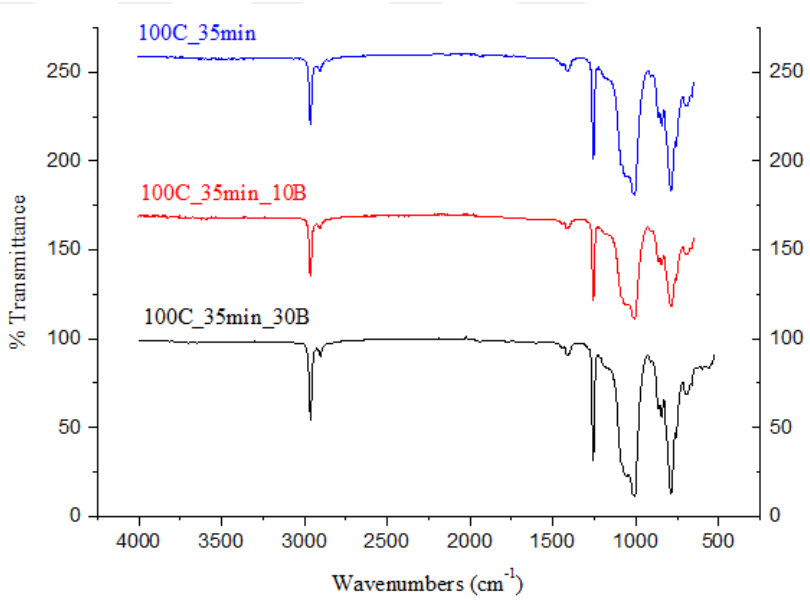

Figure 3.12 Comparable FTIR data graph to observe amount of $BaTiO_3$ effect on the bond properties

3.3.5 $BaTiO_3$ Milling

Milling process was made by using Pulverisette 7 Nano-grinding/FRITSCH as shown in figure 3.13. Process parameters were determined by FRITSCH barium titanate grinding report (FRITSCH, n.d.). $BaTiO_3$ nanoparticles were milled in two 80 ml stainless steel pots with 100 gr of ZrO_2 milling balls on each having diameter as 0.1 mm under 700 rpm. Total milling processes was lead 63 min. composed of 4 cycles. In first cycle milling time and pausing time were adjusted as 10 min and 5 min respectively. After first milling cycle the pot temperatures were checked. The pot temperatures should not exceed 80°C. Because of the increase in pot temperature the cycle times were changed as 7 min milling time and 7 min pausing time for the second cycle. Due to the heating effect, for third and fourth cycles milling time was kept as 7 min but pausing time was increased as 10 min.

a **b**

Figure 3.13 Nanogrinding device a. closed position b. open position (Personal archive, 2018)

After wet milling, the nanoparticles and milling ball mixture was dried in an oven for 2 hours at 80°C to evaporate the excess water. Then the mixture was sieved with 75 µm sieve. Because of the agglomeration between the $BaTiO_3$ nanoparticles there was no milled $BaTiO_3$ nanoparticles at the subsieve. (Adrian Bele, Cazacu, et al., 2015). Secondly the wet sieving process was examined by using 75 µm sieve again. After the mixture was put into the sieve, little amount of water was sprayed to the

mixture. Then the mixture was sieved during 60 min. After two cycle of sieving little amount of sieved $BaTiO_3$ nanoparticles were obtained. To evaporate excess water, sieved $BaTiO_3$ nanoparticles were dried in an oven. In figure 3.14 the particle size analysis of the milled nanoparticles with different milling balls and different durations were shown. The average particle sizes were given in the graphs. As seen in the graph the milled nanoparticles with 0.1 mm ZrO_2 balls and 10 mm WC balls tended to be agglomerated. According to the technical requirement of the as-received $BaTiO_3$ nanoparticles, only the particle size of nanoparticles milled with 10 mm WC balls during 30 min. was out of the range.

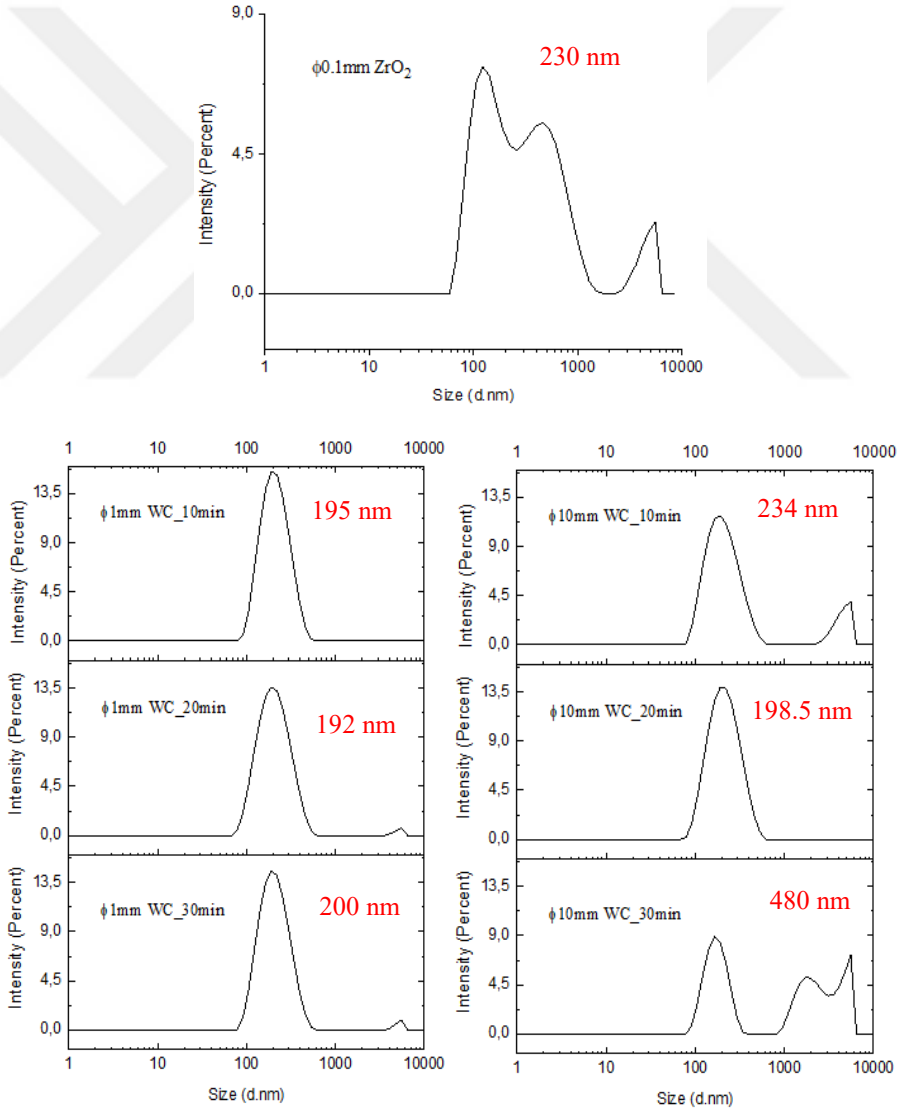

Figure 3.14 Particle size analysis of grinded $BaTiO_3$ nanoparticles

3.3.6 CNT (Carbon Nanotube) Dispersion and Coating

To obtain bilayer EAP consisting CNT layer and PDMS layer filled with $BaTiO_3$, first CNT layer should be produced. A solution was prepared with CNT and the DMF (N,N dimethylformamide) having concentration of 0.1 mg/ml. This solution was sprayed onto the metal mold. Then the mold was placed into the ultrasonic mixer to obtain homogeneously distributed CNT and to support the evaporation of the DMF solution. Because DMF solution destroys the curing mechanism of the PDMS and silicone elastomer form could not be obtained (Liu & Choi, 2012). The rest of the process was similar to the PDMS silicone elastomer production process as shown in figure 3.1. The whole process scheme is given in figure 3.15.

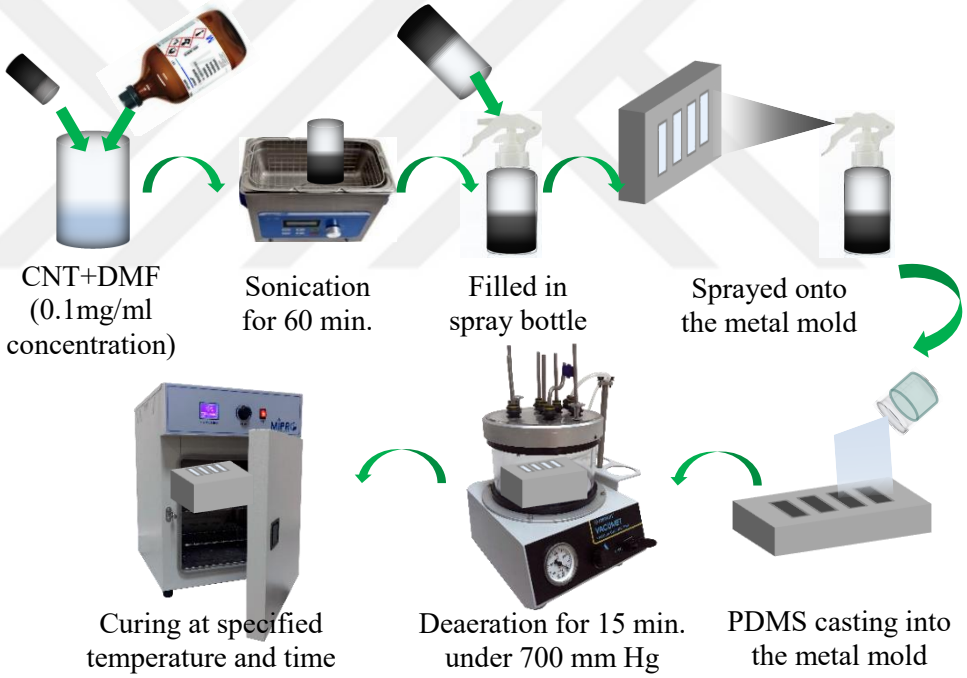

Figure 3.15 Production steps of CNT coated PDMS composite (Personal archive, 2018)

Because of the highly active surface of the CNTs, after DMF evaporation CNTs started to agglomerate to cause the non-homogeneous dispersion on the PDMS surface as shown in figure 3.16a. Additionally during the deaeration process under vacuum, because the CNTs are extremely light, with the air bubbles they penetrated through the inside of the PDMS as shown in figure 3.16b. To overcome the CNT penetration into

the PDMS spraying process was done after casting PDMS into the metallic mold. In this time because of the chemical reaction between DMF and PDMS, curing was not observed due to the reason mentioned earlier (Liu & Choi, 2012).

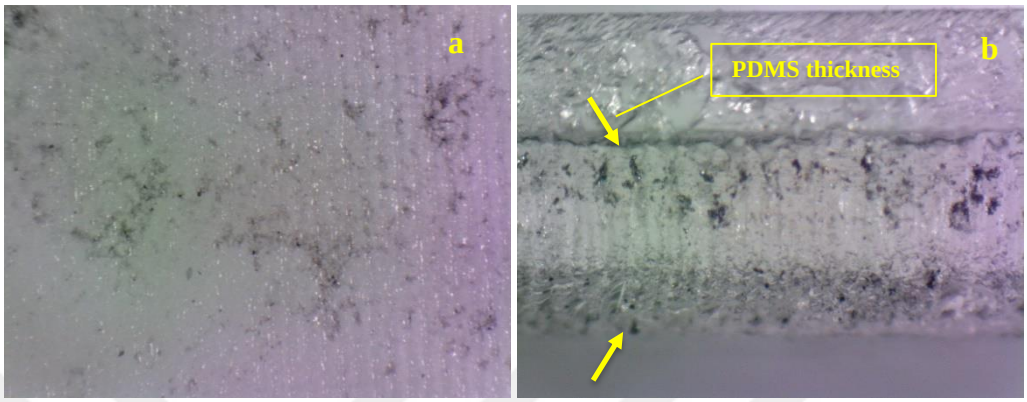

Figure 3.16 a. Agglomerated CNT on the PDMS surface b. Cross-section of the composite

Various process route combinations were tried to obtain homogeneous dispersion of CNTs with different dispersant chemicals like acetone and toluene. None of them were successful for dispersion and curing. Because of that filtration process was examined (Li, Wu, Wang, & Jiang Yadong, 2013). In this process again DMF was used as dispersant medium because it displays the best dispersing behavior with CNT (Liu & Choi, 2012). The CNT solutions having 0.1 mg/ml and 1 mg/ml CNT concentrations were prepared with DMF. Then they were put into the bath sonication for 60 min for homogeneous mixing. After that home-made setup was arranged as shown in figure 3.17. Glass petri was used to collect the excess DMF after filtration process. To filtrate the DMF from the CNT solution the filter paper was used. It was cut into appropriate shape and fixed to the glass petri. Then CNT-DMF solution was put onto the filter paper and fixed. After that it was places into the vacuum under approximately 200 mm Hg for filtration process. During the filtration, vacuum should be adjusted as constant as possible and remained low. When filtration was done, the filter paper was taken from the glass petri and put into an oven at 60°C for 30 min to evaporate the excess DMF. After drying, pure PDMS sample or PDMS composite sample containing $BaTiO_3$ nanoparticles was stamped to the filter paper to get CNT layer with approximately 2.5 kg pressure. The process scheme was shown in figure 3.18.

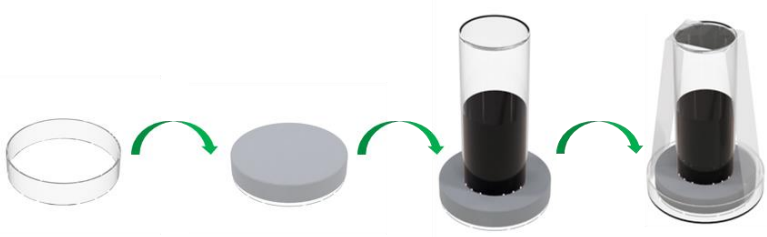

Figure 3.17 CNT filtration set-up schematization

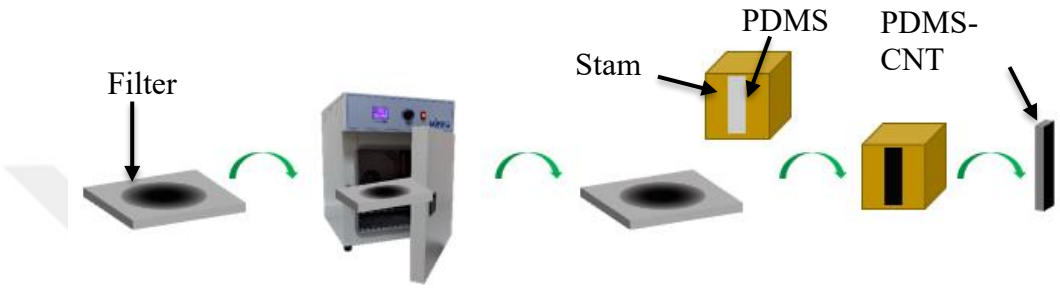

Figure 3.18 CNT stamping process and the PDMS composite coated CNT layer (Personal archive, 2018)

For this stamping process, 100C_35min PDMS and 100C_35min_10B samples were used. In figure 3.19, digital microscope images were given of neat PDMS, PDMS with $BaTiO_3$ composite and samples coated with CNT layer. Due to the digital microscope images, homogeneous dispersion of CNTs was obtained by this method as shown in figure 3.20-a. To achieve denser CNT layer, the CNT-DMF solution having 1 mg/ml concentration was used. The comparison of the solution having 0.1 mg/ml CNT concentration and solution having 1 mg/ml CNT solution was given in figure 3.20. As shown in the figure 3.20-b CNT layer containing more CNT concentration was fragmentally oriented. This could be because of the highly reactive surface of CNTs. The cross-sectional microscope image of the 100C_35min_10B sample was shown in figure 3.21. The $BaTiO_3$ nanoparticles was observable as white regions with the CNTs as black regions.

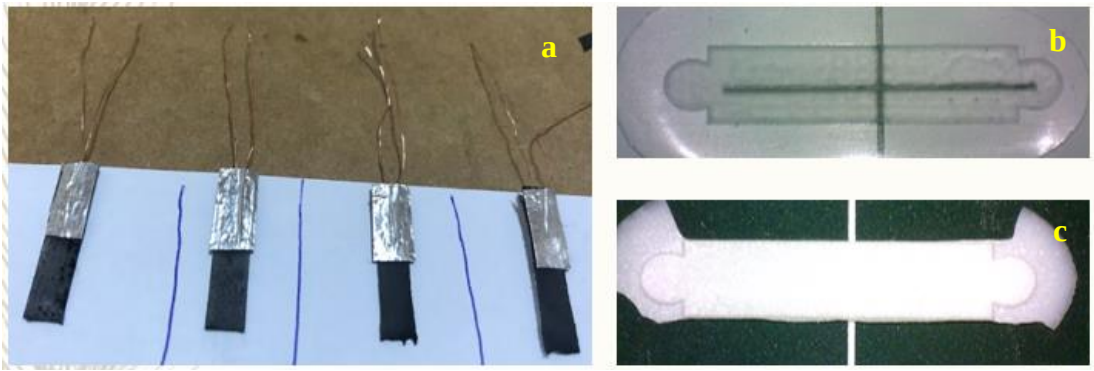

Figure 3.19 a. samples coated with CNT layer b. neat PDMS c. PDMS with $BaTiO_3$ composite

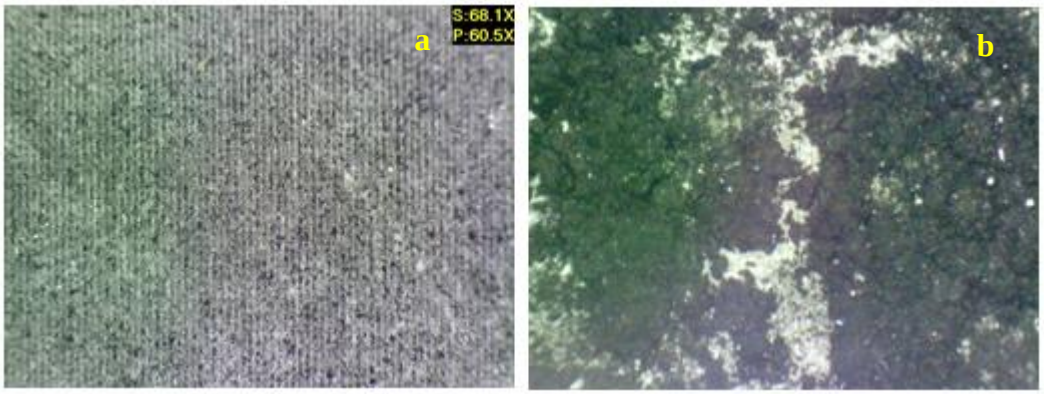

Figure 3.20 Surface of the PDMS a. coated by CNT solution having 0.1 mg/ml concentration b. coated by CNT solution having 1 mg/ml concentration

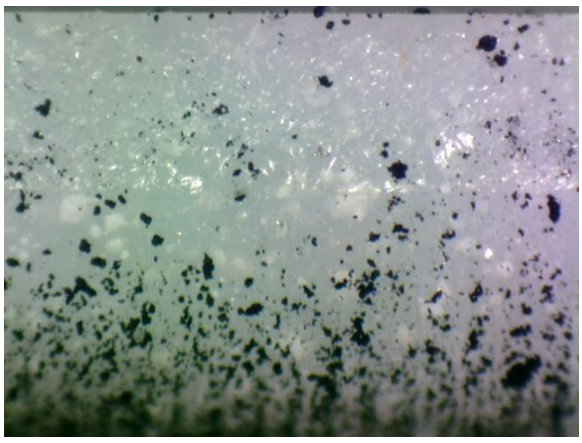

Figure 3.21 Cross-sectional image of 100C_35min_10B PDMS composite sample

To achieve optimum CNT dispersion on the surface the CNT-DMF solution having 0.4 mg/ml CNT concentration was prepared. For this stamping process 150C_10min and 40C_4h PDMS samples were used. As seen in the figure 3.19-a, the PDMS samples cured at lower temperature were stamped well compared with the PDMS samples cured at higher temperature.

LCR meter measurement was done on the samples coated with CNT to examine CNT effect to the dielectric constant. The results were shown in figure 3.22. Because of the less concentration of CNT the dielectric constants of samples stamped with solution having 0.1 mg/ml CNT concentration have smaller values. Due to the same reason the highest dielectric constant of 5.68×10^{-24} was reached with solution having 1 mg/ml CNT concentration.

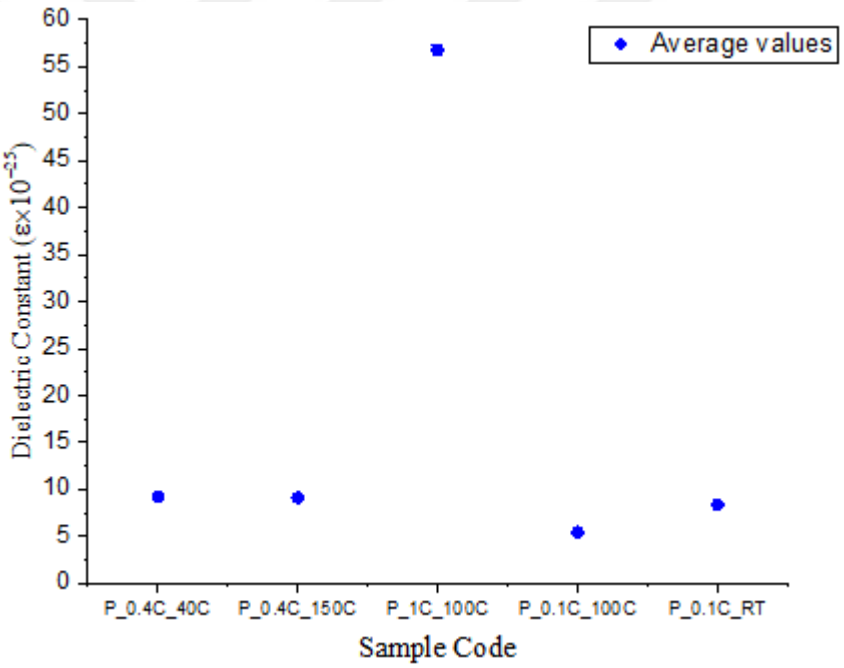

Figure 3.22 CNT effect on dielectric constant

3.3.7 Electroactive Properties

To measure electroactive response, conductive copper wires were used to make a circuit. First these wires were attached to the composite surface by silver conductive paste. Because of the smoothness of the neat PDMS surface which is not coated with CNT, adhesion of silver conductive paste was difficult. Due to this, aluminum foil

band was used to stabilize copper wire to the neat surface of PDMS. The schematization is given in figure 3.23.

Figure 3.23 Contact schematization of PDMS-CNT composite

To obtain electroactive response set-up was constructed with power supply as shown in figure 3.24. For activation 10-30 V DC voltage range was used. Response was observed with the digital microscope.

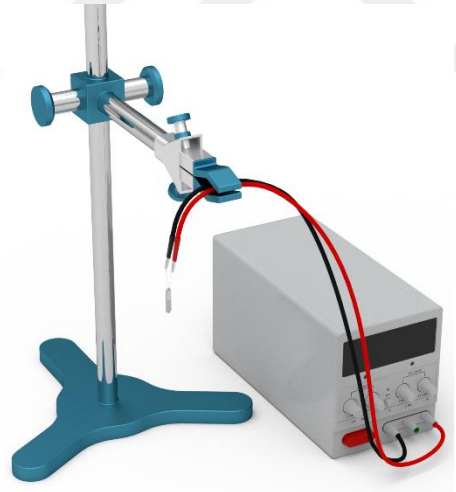

Figure 3.24 Schematization of electrical actuation process

At the end of the measurement, no electric response was obtained. One of the possible reason is that thickness difference between the CNT layer and the PDMS. According to the Hu et al. research in 2014 with the spongy graphene, PDMS thickness has crucial impact on the electrical response. The thickness of PDMS affects the heat

distribution and also the thinner the PDMS layer the easier to bend (Y. Hu, Lan, Wu, Zhu, & Chen, 2014).

A voltmeter was used to measure electrical conductivity of stamped CNT layer. Voltmeter and the power supply were connected to the sample. By applying voltage to the sample, same voltage value was observed at the voltmeter as shown in figure 3.25. The experiment was performed with different samples. Nearly all CNT layers were conductive except CNT layers produced by solution with 0.1 mg/ml concentration. The reason could be the insufficient CNT concentration to conduct electricity.

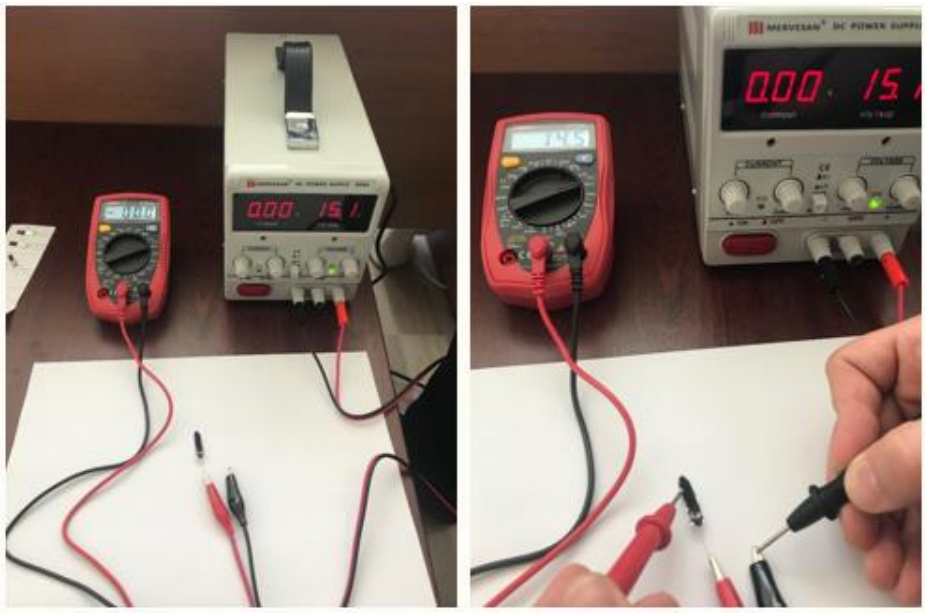

Figure 3.25 Electrical conductivity measurement (Personal archive, 2018)

CHAPTER FOUR
CERAMICS: PIEZOELECTRIC CERAMICS

4.1 Ceramics

The word “ceramic” comes from the Greek word “keramos” meaning “burned thing” or “pottery”. Until ancient times people made stuffs from clay by burning them with fire. Generally there is no specific explanation about what the ceramic is. During for long time many ceramic scientists tried to describe the ceramic in terms of their properties, production methods, application areas or their chemistries. Richerson (2000) defines ceramics as “most solid materials that aren’t metal, plastic, or derived from plants or animals are ceramics.” However the most general and acceptable definition is made from Kingery at 1976 which is “a ceramic is a nonmetallic, inorganic solid.” (Carter & Norton, 2007; Richerson & Lee, 2018).

Ceramics are made of metallic and nonmetallic elements bonding together. This bonding type could be ionic, covalent or both but mostly be ionic. Because of that it could be said that ceramics are made of ions instead of atoms. The ions which charged positively are metals and called cations. The negatively charged ions are non-metals and called as anions. The material properties of ceramics mainly depend on these ions in terms of electrical charge magnitude and ion radius (Callister & Rethwisch, 2014).

The overall electrical charge of ceramic material should be zero. Therefore ionic charge of the components should be balanced and it determines the chemical formula. For example consider TiO_2. Because the titanium cation has ionic charge as (+4), there should be two oxygen anion having (-2) ionic charge to balance the titanium cation. Additionally this cation to anion radius ratio defines the coordination number and geometry. Generally cations tend to have smaller radius than anions. Therefore r_c/r_a ratio (cation to anion radius ratio) is generally smaller than unity. Cations are placed tetrahedral, octahedral or cubic sites, if they have coordination number as 4, 6 and 8 respectively. The defined coordination numbers and geometries according to r_c/r_a ratio are given in the figure 4.1 (Callister & Rethwisch, 2014).

Coordination Number	*Cation–Anion Radius Ratio*	*Coordination Geometry*
2	<0.155	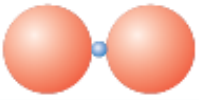
3	0.155–0.225	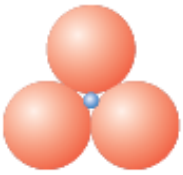
4	0.225–0.414	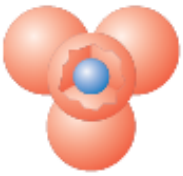
6	0.414–0.732	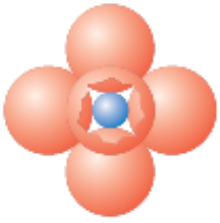
8	0.732–1.0	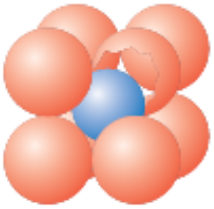

Figure 4.1 Coordination numbers and geometries for various cation–anion radius ratios (r_C/r_A) (Callister & Rethwisch, 2014)

4.1.1 Traditional Ceramics

Despite how hard to classify ceramics, they could be separated into two main groups as traditional and advanced ceramics. Traditional ceramics have very broad application areas like bricks and tiles, sanitary ware, kitchenware, refractories etc. (Carter & Norton, 2007).

Production of traditional ceramics usually begins with the slurry having different kind of raw materials like clay, kaolin, quartz, feldspar and some additives to make production and the final product properties better. Clay and kaolin are nearly the same.

Kaolin is the pure form of the clay and has a chemical formula as $Al_2O_3 \cdot 2SiO_2 \cdot 2H_2O$. They are generally used to provide plasticity to the slurry when they are mixed with water. Quartz is the SiO_2 source and used for providing rigidity, high temperature and fracture resistance to the final product (Callister & Rethwisch, 2014; Carter & Norton, 2007; Reed, 2008; Richerson & Lee, 2018).

Feldspar is used for to create flux during sintering process. It melts before the silica sources and helps the particles to be sintered. There are three types of feldspar: K-feldspar ($K_2O \cdot Al_2O_3 \cdot 6SiO_2$) which is called orthoclase, Na-feldspar ($Na_2O \cdot Al_2O_3 \cdot 6SiO_2$) which is called albite and anorthite ($CaO \cdot Al_2O_3 \cdot 2SiO_2$). Then the slurry is poured into a mold which is made of plaster of Paris or polymer depending on the process type. The desired shape even if it is complex could be given by this process and it is called slip casting. After casting the slurry into the mold, it takes time to drain water from the slurry into the mold to get green body shape. If it is desired that the inside of the object is hallow; after the green body part has desired thickness, the remaining slip could be drained. Green body means the product before sintering. It should be rigid enough to sustain any external stress during transportation until sintering. Finally, the green body is sintered at temperature and time specified by the process parameter. Sintering regime depends on the production method and final product properties (Callister & Rethwisch, 2014; Carter & Norton, 2007; Reed, 2008; Richerson & Lee, 2018). The general steps of hallow slip casting process is given in figure 4.2.

Figure 4.2 Basic steps of hallow slip casting (Personal archive, 2018)

4.1.2 Advanced Ceramics

Advanced ceramics are excepted high technology materials compared to traditional ones. They have superior properties as high thermal, mechanical, electrical, optical and magnetic properties. Also they have high temperature and corrosion resistance (Carter & Norton, 2007).

Advanced ceramics are gathered into six sub-groups which are structural ceramics, electronic ceramics, bioceramics, coatings and thin films, composites and nanoceramics. Structural ceramics are used in armors, cutting tools, heat exchangers and motor engines. SiC, Si_3N_4, B_4C and Al_2O_3 could be given as examples of structural advanced ceramic raw materials. The properties like high hardness, high temperature, corrosion and creep resistance are their main requirements. Their main disadvantage is very high production cost (Callister & Rethwisch, 2014; Carter & Norton, 2007).

Electronic ceramics are used in dielectric capacitors, piezoelectric devices, sensors and microelectromechanical devices (MEMs). Their main raw materials are $BaTiO_3$, lead-zirconate-titanate (PZT) and ZnO etc. They have special type of structures and working mechanism in crystallographic base. High electrical and magnetic properties are expected from this type of materials. The main disadvantage is the small size as in

microns. Because of the micron size the production, reproducibility and maintain the desired properties are difficult to sustain (Callister & Rethwisch, 2014; Carter & Norton, 2007; Dascalu & Maugin, 1995; Zhu, 2009).

Bioceramics are used in human-body. Therefore their requirements are a bit different from others like biocompatibility, biodegradability and nontoxicity. Al_2O_3 and ZrO_2 could be given as examples of bioceramics but the main bioceramic is the hydroxyapatite. It has a structure nearly as same as the human bones. The main difficulty is that they should be compatible to human body (Callister & Rethwisch, 2014; Carter & Norton, 2007).

Coating and thin films are used modify the surface properties of the main material. By coating the material with some specific materials, new properties could be given like anti-bacterial, frictionless or bio-active surface properties. There are some parameters should be considered during the coating process like adhesion, lattice mismatch between the thin film and the substrate, durability of the coating etc (Callister & Rethwisch, 2014; Carter & Norton, 2007).

Some ceramics are also used to make composites like ceramic-matrix-composites (CMCs) and metal-matrix-composites (MMCs). Using ceramics as matrix or reinforcement material could give the overall material some superior properties like high strength, high wear, corrosion or fatigue resistance (Callister & Rethwisch, 2014; Carter & Norton, 2007).

Recently, nanoceramics are one of the most popular advanced ceramic materials. Especially their production is the main challenge. As the dimensions get smaller in nano size, control of the properties and stabilities of nanomaterials get harder. They are used in high-tech applications like space technologies, electronic and magnetic devices, reinforcements and even in cosmetics as sunscreens. Because of the volatility of the dust, the process conditions should be optimized carefully. The most popular nanoceramics are nanocarbons as carbon nanotubes, graphenes and fullerenes

(Callister & Rethwisch, 2014; Carter & Norton, 2007; Pietroiusti, Stockmann-Juvala, Lucaroni, & Savolainen, 2018).

Production methods of advanced ceramics are different from the traditional ceramics. These differences are given in figure 4.3.

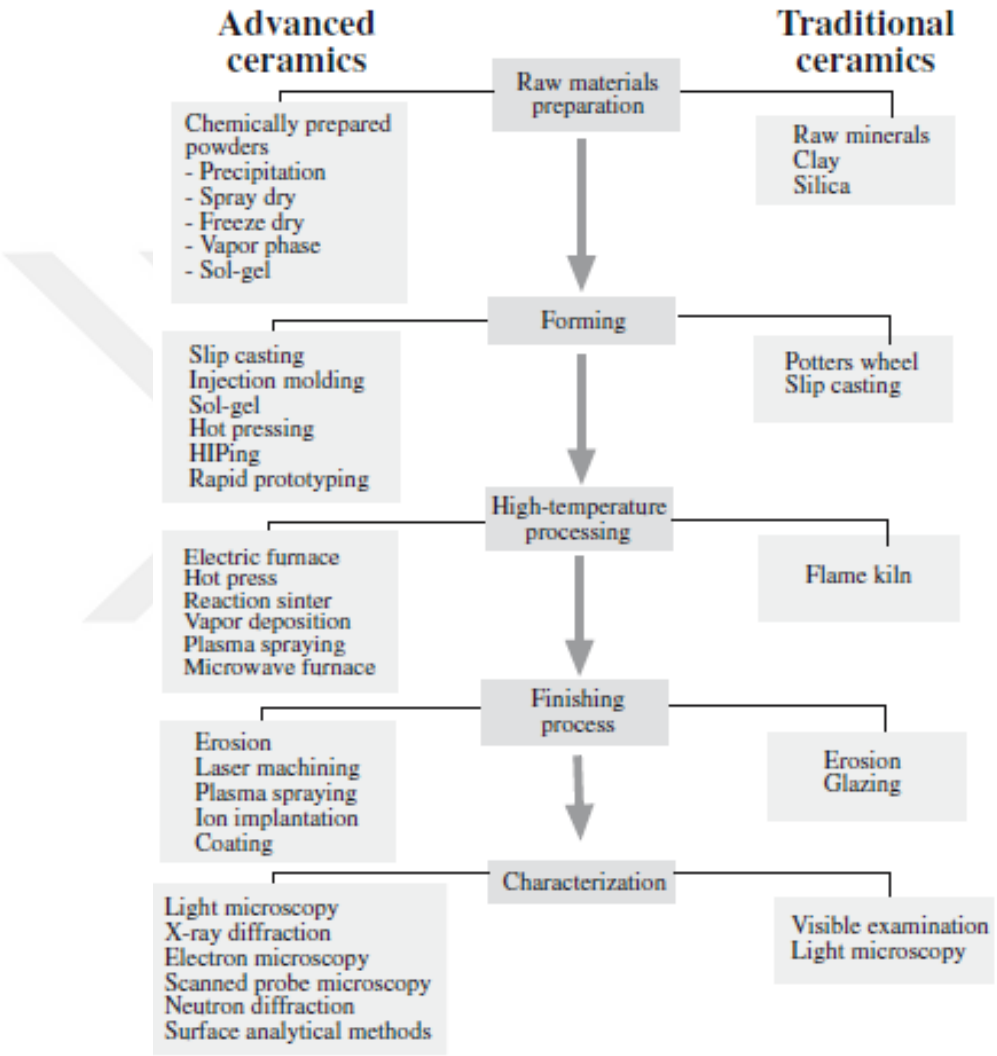

Figure 4.3 Production method scheme of advanced and traditional ceramics (Carter & Norton, 2007)

4.2 Piezoelectricity

The scope of this thesis is focused on $BaTiO_3$ which is used in electrical advanced ceramic applications. Therefore before explaining piezoelectricity, there should be some key words that have to be mentioned. Dielectric means that electrically insulated

material containing electric dipoles (Callister & Rethwisch, 2014). Paraelectric means that electric dipoles exist only under applied electric field (Carter & Norton, 2007). Piezoelectric means that material could convert electrical energy into the mechanical energy or vice versa (Callister & Rethwisch, 2014). Pyroelectricity means that materials could create electrical energy with thermal energy instead of mechanical energy (Richerson & Lee, 2018). Ferroelectricity is sub-class of the piezoelectricity and has permanent dipoles whether there is an electrical field or not. Non-ferroelectricity means that materials are piezoelectric but not having permanent dipoles (Trolier-Mckinstry, 2008; Zhu, 2009).

4.2.1 Polarization

$BaTiO_3$ is one of the important dielectric ceramics. It has perovskite structure and this means its dipoles could change according to the electric field and become polarized. Polarization is mainly the base of the piezoelectric and ferroelectric effect. There are four different types of polarization (Carter & Norton, 2007).

In the presence of electric field the electrons located around the nucleus begin to move through the positive side of the field still keeping their position near the nucleus shown in figure 4.4. It is called electric polarization and all materials could display this kind of polarization because all materials are composed of atoms. In electric polarization atoms behave like temporarily induced dipoles. This polarization has relatively small magnitude because the distance between the positive and the negative sides of the atom is very small. Materials which are covalently bonded and not having permanent dipoles like diamond and silicon have only electronic polarization (Carter & Norton, 2007).

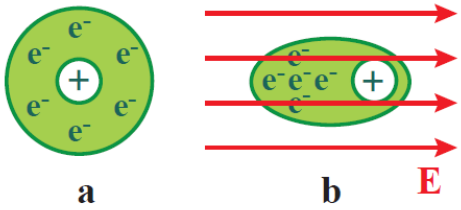

Figure 4.4 Electric polarization scheme a. without electric field b. with electric field

Second type of polarization is the ionic polarization. It occurs between ionically bonded materials as most of the ceramics. When an ionic bond exposed to electric field, it starts to expand or contract depending on the field direction shown in figure 4.5. Ionic bonds behave like temporarily induced dipoles. Also ionic polarization has small magnitude because of the same reason as electric polarization (Carter & Norton, 2007).

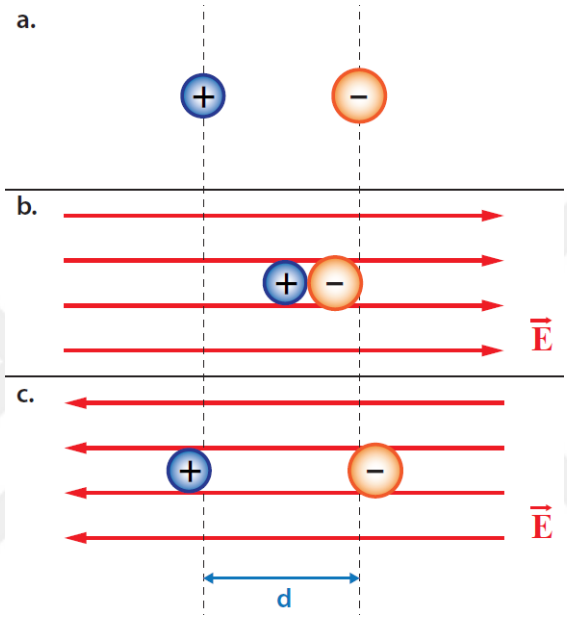

Figure 4.5 Ionic polarization scheme a. without electric field b. with electric field c. with electric field in the opposite direction

Third type of polarization is the dipolar polarization. Permanent dipoles force the material to change its structure, when they are exposed to electric field. Because of that, very few materials show this kind of polarization. Among them $BaTiO_3$ is the most important one. Because of the polymorphic transformations, presence of electric field, Ti^{4+} changes its position and the structure become polarized shown in figure 4.6 (Carter & Norton, 2007).

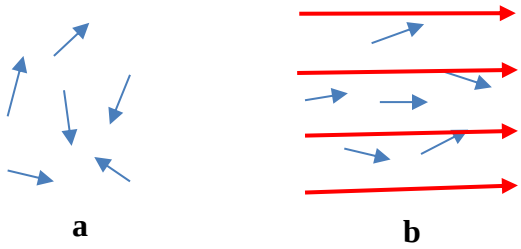

Figure 4.6 Dipolar polarization scheme a. random dipole orientations without electric field b. aligned dipole orientation with electric field

Impurities in structures cause some interfaces like grain or phase boundaries and free surfaces. Because of that charges could move on the surface, when electric field is applied shown in figure 4.7. It is called interfacial polarization. Although the mechanism under this polarization is not well explained, it is very common. Because most real materials are not pure and having impurities into their structures (Carter & Norton, 2007).

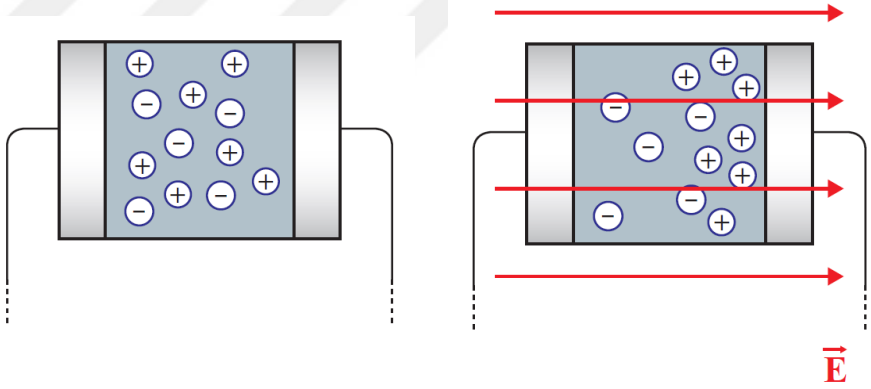

Figure 4.7 Interfacial polarization scheme a. without electric field b. with electric field

4.2.2 Dielectric Behavior

Most of the ceramics are dielectric insulators. They do not conduct electricity but could store them in a specific manner. This behavior forms the basis of the capacitors. It is based on the polarization behavior. Polarization mainly depends on the electric dipoles. An atom is electrically stable in normal conditions as shown in figure 4.8. Because of the interactions between neighboring atoms they become polar and create dipoles (Callister & Rethwisch, 2014; Richerson & Lee, 2018).

Figure 4.8 Electric dipoles scheme a. unpolarized b. polarized

4.2.3 Piezoelectric Ceramics

Piezoelectricity became an important research field at 1800s by Curie brothers. During World War I, rapid improvement was achieved in piezoelectric materials and at 1921 by Valasek who discovered ferroelectricity concept and Rochelle salt showing ferroelectric behavior. Rochelle salt was the first ferroelectric material. However it has a disadvantages about production because its ferroelectric properties was destroyed in little amount of crystal orientation change (Dascalu & Maugin, 1995).

The first discovered piezoelectric ceramic is potassium dihydrogen phosphate (KDP) at 1935 by Busch and Scherrer (Zhu, 2009). In 1945, by discovery of $BaTiO_3$ the application areas of piezoelectric ceramics were expanded like acoustic wave devices, microphones and speakers, actuators, sensors, ignition generators, smart structures, energy harvesting devices etc. (Dascalu & Maugin, 1995; Zhu, 2009). In 1950s a new class of piezoelectric material was found by Jaffe et al. which is called lead-zirconate-titanate (PZT) having the highest dielectric properties (Zhu, 2009).

Piezoelectricity means that a material could create electrical energy when it is exposed to stress or change its shape upon applied electrical field. Literally it means “pressure electricity”. Depending on the applied stress or the magnitude and the sign of the electrical field, output properties could be changed. There are two types of piezoelectric effect which is called direct and inverse effect. In direct effect, electrical output could be obtained by applied stress shown in figure 2.9. There are electrodes on top and the bottom of the dielectric materials shown as brighter color. Applying on tension or compression on the material, electrical output is obtained and the light bulb starts lighting up. On the other hand in inverse effect, the shape of the material could

be changed by applying electric field. This mechanism is shown in figure 4.9. Depending on the electric field direction, the material could expand in longitudinal direction and shrink in the lateral direction (Carter & Norton, 2007; Richerson & Lee, 2018).

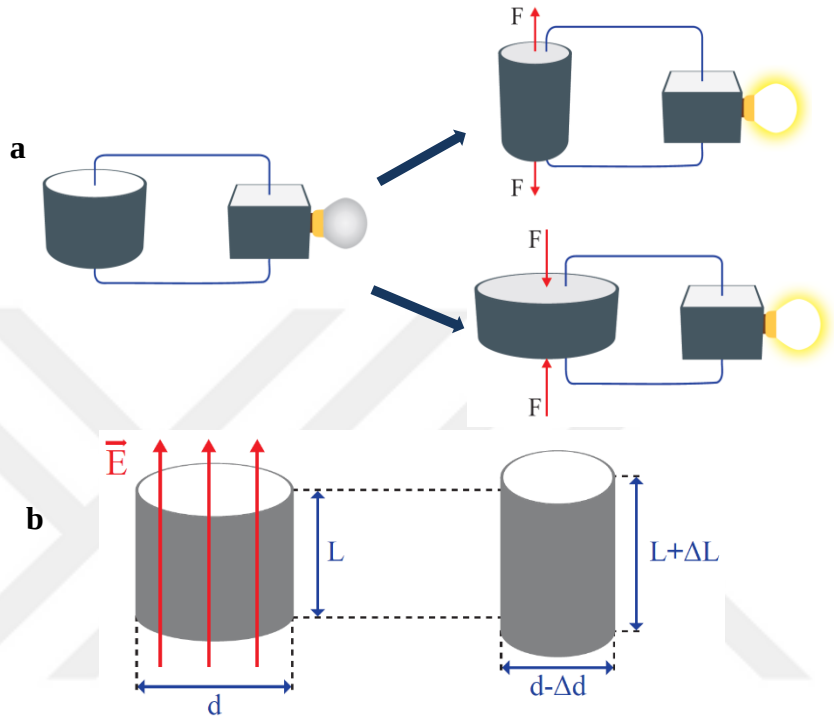

Figure 4.9 a. direct piezoelectric effect b. indirect piezoelectric effect

Pyroelectricity is the subclass of the piezoelectricity. “Pyro” comes from Greek and it means “fire”. Therefore literally pyroelectricity means “fire electricity”. As in piezoelectricity, pyroelectric materials have spontaneous polarization and their dipoles are activated with thermal stimulation instead of mechanical stress. Generally they are used as thermal sensors where small dimensions are required (Richerson & Lee, 2018).

Some materials have polarization due to permanent dipoles without applied electrical field. These are called ferroelectric materials. As in piezoelectricity for ferroelectricity, the material should have non-centrosymmetric structure. Imagine a single crystal having around 100µm in diameter. All atoms are positioned at specific positions to create the smallest unit of the structure which is called unit cell. Repeating symmetries of these unit cells in some defined ways creates whole material structure. Due to these symmetries 32 symmetrical groups reveal and these defines the material

as piezoelectric or not. Only 21 groups in 32 symmetry point groups are non-centrosymmetric and possess piezoelectric properties. Subgroups of these 21 symmetry point groups also possesses piezoelectric and pyroelectric properties as shown in figure 4.10. Some of these pyroelectric materials possess ferroelectric behavior which their domain could be reoriented by the electric field (Carter & Norton, 2007; Richerson & Lee, 2018; Trolier-Mckinstry, 2008; Zhu, 2009).

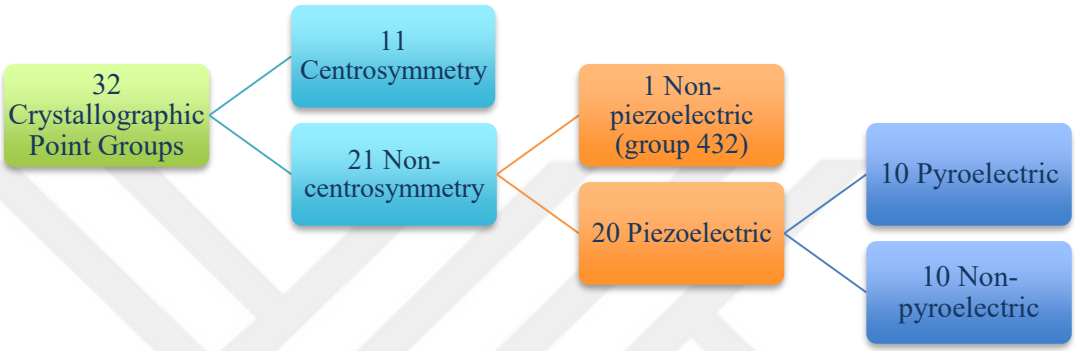

Figure 4.10 32 symmetry point group scheme (Trolier-Mckinstry, 2008)

There are some important materials showing piezoelectric behavior but not ferroelectric. These materials have wurtzite type structure. Their polarization is permanent and could not be reoriented (Richerson & Lee, 2018; Trolier-Mckinstry, 2008). Zinc oxide (ZnO) is one of the material having wurtzite structure and its crystal structure is shown in figure 4.11 as same as quartz.

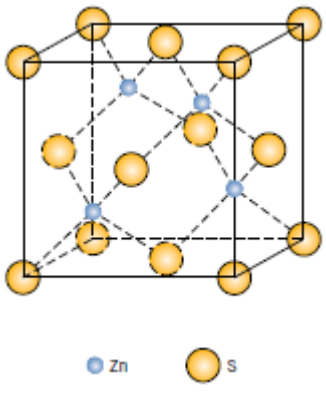

Figure 4.11 Wurtzite structure (Callister & Rethwisch, 2014)

4.2.3.1 Natural

Piezoelectric ceramics are divided into two groups. One of this group is natural piezoelectric ceramics. These are naturally occurring generally single crystal ceramics like quartz, Rochelle salt, topaz, tourmaline-group minerals etc. The simple SiO_2 tetrahedron structure is shown in figure 4.12 (Dascalu & Maugin, 1995).

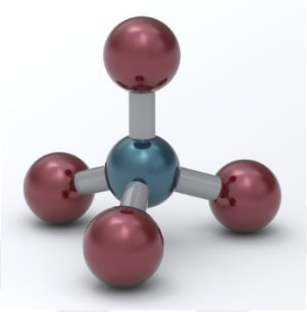

Figure 4.12 Simple SiO_2 tetrahedron

4.2.3.2 Synthetic

Other type of piezoelectric ceramics is synthetic, man-made materials. Generally they have ABO_3 perovskite type crystal structure like barium titanate ($BaTiO_3$), lead-zirconate-titanate (PZT), potassium niobate ($KNbO_3$) etc. (Dascalu & Maugin, 1995). Structure of these man-made piezo-ceramics is given in figure 4.13.

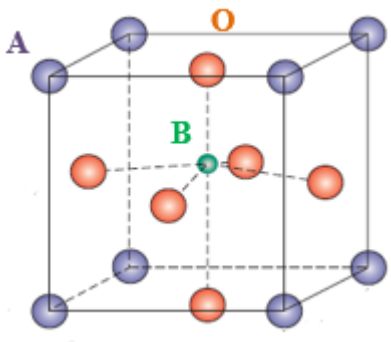

Figure 4.13 Example of piezo-ceramic structure (Callister & Rethwisch, 2014)

4.3 Barium Titanium Oxide ($BaTiO_3$)

$BaTiO_3$ has great attention due to its very high dielectric constant. Recent researches are about composites having various forms of $BaTiO_3$ as nanoparticles (Xie et al., 2005), nanocrystals (Ali, Yu, Duan, Yu, & Zhu, 2017), nanowire (Choi, Choi, Yang, Kim, & Yu, 2016) and multipods (Nayak et al., 2014).

Due to the technological development, requirement of more compact electrical devices necessitate new materials. Due to these necessities composite materials are developed especially used in applications as capacitors, transducers and energy storage devices. Because of its high dielectric properties $BaTiO_3$ satisfies all requirements. However in low dimensions, it is difficult to fulfill high electrical properties. Therefore polymer-ceramic composites arisen (Ali et al., 2017).

Basically composites are made of two components: matrix and reinforcement. In polymer-ceramic composites, there are properties of both ceramics and polymers, better dielectric properties from ceramics and elasticity, producibility and lightweight from polymers. Also properties could be adjustable according to the reinforcement percent and production method (Bai et al., 2000; Xie et al., 2005).

$BaTiO_3$ are produced by different methods like solid-state reactions, chemical synthesis or hydrothermal synthesis. Kiss et al. (1966) used two different methods to produce $BaTiO_3$. First is isothermal pyrolysis method by using barium titanyl oxalates or mixed calcium-barium titanyl oxalates. Secondly they used titanate esters hydrolysis in barium hydroxide (Kiss, Magder, Vukasovich, & Lockhart, 1966). Xia et al. (1995), Clark et al. (1999), Hakuta el al. (2005) and Özen et al. (2012) produced $BaTiO_3$ by using hydrothermal synthesis (Clark, Takeuchi, Ohtori, & Sinclair, 1999; Hakuta, Ura, Hayashi, & Arai, 2005; Özen, Mertens, Schroeven, Snijkers, & Cool, 2012; Xia, Shi, Zhong, & Guo, 1995). Zhou et al. (1997) and Kobayashi et al. (2004) used sol-gel method to produce $BaTiO_3$ thin film embedded silver nanoparticles (Kobayashi, Nishikata, Tanase, & Konno, 2004; Zhoul, Li, Gui, Zhang, & Barber, 1997). Maison et al. studied catecholate process to get nanoscale $BaTiO_3$ (Maison,

Kleeberg, Heimann, & Phanichphant, 2003). Malghe et al. (2004) used microwave heating process as different from each other to produce cubic $BaTiO_3$ powder (Malghe et al., 2004). Al-Shakarchi & Mahmood (2011) obtained $BaTiO_3$ by using three different chemical method as Sodium hydroxide-ethanol method, oxalate method and sodium hydroxide method (Al-Shakarchi & Mahmood, 2011). De Andrade et al. used solid-state reactions to produce barium titanate (de Andrade, Carneiro, Moreira, Araújo, & Moraes, 2014).

4.3.1 Dielectric Constant

Dielectric materials have a certain level to sustain the applied field. This level is called dielectric strength. Dielectric strength should be high for especially for the very thin dielectric materials (Carter & Norton, 2007).

Dielectric constant is the charge storage capacity for especially capacitors. It is related with the stored charge per unit area at the same time with the applied electric field with a constant. This constant is called dielectric constant or permittivity. If there is two parallel plate, the permittivity between these plates is the vacuum permittivity which is 8.85×10^{-12} $F.m^{-1}$. When a dielectric material is placed between them, the charge storage capacity is affected by the dielectric constant of this dielectric material. It means that the higher the dielectric constant of the dielectric material, the higher the charge which is stored on the capacitor. This is the main working principle of the capacitors. Simple capacitor schematic is shown in the figure 4.14 (Carter & Norton, 2007).

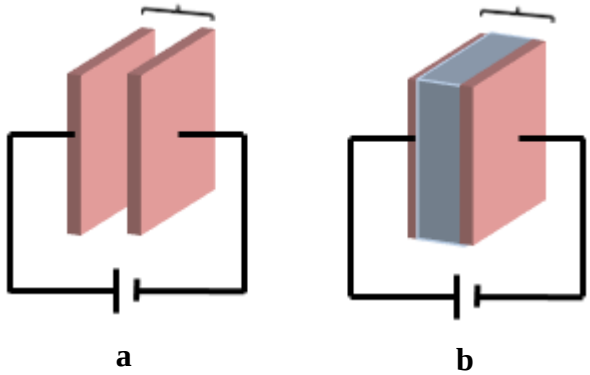

Figure 4.14 General scheme of capacitor a. air between the capacitor plates b. dielectric material between the capacitor plates

4.3.2 Crystal Structure

The typical $BaTiO_3$ perovskite structure is given in figure 4.15. $BaTiO_3$ leaded a ABO_3 ferroelectric perovskite crystal structure class (Zhu, 2009). Ba^{2+} ions are located at the corners having coordination number 12. Ti^{4+} ions are located at the octahedral position as a center of the structure having coordination number 6. And O^{2-} ions are located at the face position having coordination number 6 (Callister & Rethwisch, 2014).

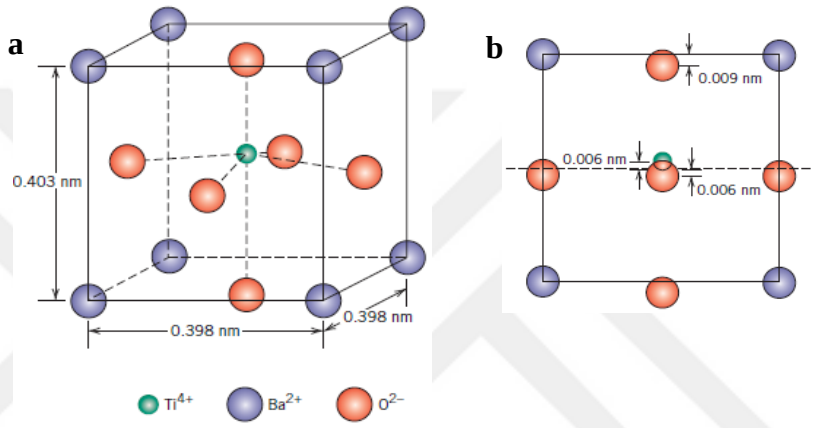

Figure 4.15 a. Perovskite crystal structure and location of the Ti^{4+} ion in the octahedral site b. polarization effect on Ti^{4+} (Callister & Rethwisch, 2014)

$BaTiO_3$ has four polymorphic transformation shown in figure 4.16. Below its Curie temperature (T_c) which is 120°C, $BaTiO_3$ shows ferroelectric behavior because of the polymorphic phase transformation. Ti^{4+} ions slightly change their TiO_6 octahedral positions below the T_c. This causes a change in crystal structure from cubic to tetragonal. While the cubic form of $BaTiO_3$ is paraelectric, tetragonal form is ferroelectric. Therefore, in the presence of electrical field below T_c, Ti^{4+} ions oscillate back and forth, change dipoles and because of that piezoelectric effect is created (Ali et al., 2017; Carter & Norton, 2007; Clark et al., 1999). The polarization effect and the position of Ti^{4+} and O^{2-} are shown in the figure 2.15 (Callister & Rethwisch, 2014).

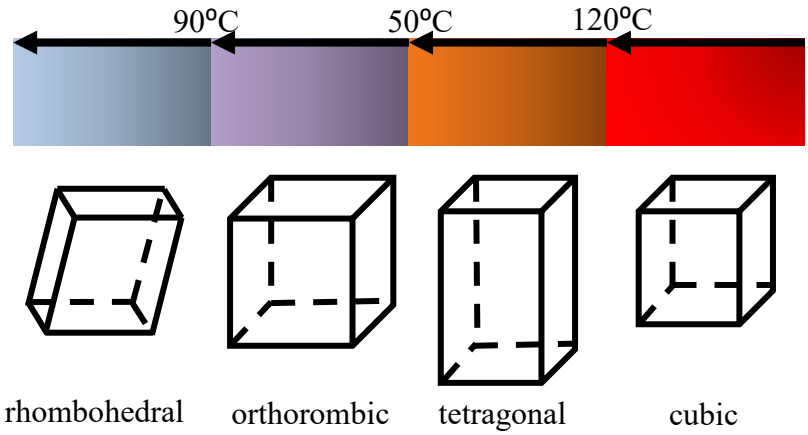

Figure 4.16 Polymorphic transformation of $BaTiO_3$

CHAPTER FIVE
CONCLUSIONS

In this study, PDMS and MWCNT layered composite structure is studied for the production of EAP. Within the carried experimental studies, optimum curing condition of PDMS to produce crack-free surface with the highest dielectric constant as $5.09x10^{-25}$ is found for the PDMS cured at 100°C for 35 min. During the optimization of PDMS, curing conditions have not affected the molecular structure of PDMS according to results of FTIR analysis. To develop dielectric properties of PDMS based EAP, several $BaTiO_3$ ratios are mixed to PDMS to form a PDMS/$BaTiO_3$ nanocomposite.

Optimum curing conditions were determined as 100°C 35 min. having crack-free surface and high dielectric constant. No significant effects of curing parameters on the bond properties were observed. By increasing the $BaTiO_3$ content, the dielectric constant is increased until 1wt %. After 1wt %, dielectric constant begins to decrease. This is related with the percolation threshold values described in the other researches in literature mentioned in chapter 4.3.4. Because of the highly dominant nature of the PDMS and very little amount of $BaTiO_3$ in it, overlapping the transmittance values of the $BaTiO_3$ with the PDMS could be occurred according to the FTIR results.

Due to agglomeration of $BaTiO_3$ nanoparticles, dry sieving process could not be succeeded. To overcome this, wet sieving was examined. In water medium, sieve having 75 µm sieving size was used to sieve the $BaTiO_3$ nanoparticle from the ZrO_2 milling balls. At the end of sieving, little amount of $BaTiO_3$ nanoparticles were obtained. According to the particle size analysis results, the average particle size of nanoparticles was 230 nm. Instead of agglomeration, particle size was still in the ranges asserted in the technical data sheet of $BaTiO_3$.

For production of CNT layer by spraying method two different solution having different CNT concentration were prepared as 0.1 mg/ml and 1 mg/ml. After spraying the curing process was negatively affected by the interaction between DMF and PDMS. Therefore stamping process was conducted as a solution. To produce CNT

layer for stamping three different solution having different CNT concentration were prepared as 0.1 mg/ml, 0.4 mg/ml and 1 mg/ml. Optimum dispersion was obtained at solution having 0.4 mg/ml CNT concentration. Additionally it was observed that the samples cured at lower temperatures stamped easily than the samples cured at higher temperatures.

To measure electroactive response a setup was conducted by using copper wires and aluminum tape. The DC voltage was applied between 0-30 V during approximately 5 min. Because of the thickness of the PDMS, the mechanical force created by the shrinkage of CNT layer due to the thermal energy was not sufficient to bend the PDMS layer.

To confirm the electrical conductivity of the stamped CNT layers power supply was connected to the samples with the voltmeter. Same voltage values were observed at the power supply and the voltmeter for samples having stamped layer by solutions 0.4 mg/ml CNT concentration and 1 mg/ml CNT concentration. From 0.1 mg/ml solution was insufficient to create a conductive stamped CNT layer.

Optimization of LCR meter having uniform pressure and electroactive response of the PDMS composite studies could be done as future studies in the scope of this dissertation.

REFERENCES

Al-Shakarchi, E. K., & Mahmood, N. B. (2011). Three Techniques Used to Produce BaTiO3 Fine Powder. *Journal of Modern Physics*, *2*, 1420–1428.

Ali, D., Yu, B., Duan, X., Yu, H., & Zhu, M. (2017). Enhancement of output performance through post-poling technique on BaTiO3/PDMS-based triboelectric nanogenerator. *Nanotechnology*, *28*, 075203.

Andersson, L. H. U., & Hjertberg, T. (2003). Silicone Elastomers for Electronic Applications. I. Analyses of the Noncrosslinked Fractions. *Journal of Applied Polymer Science*, *88*, 2073–2081.

Bai, Y., Cheng, Z. Y., Bharti, V., Xu, H. S., & Zhang, Q. M. (2000). High-dielectric-constant ceramic-powder polymer composites. *Applied Physics Letters*, *76*(25), 3804.

Bar-Cohen, Y. (2004). *Electroactive Polymer (EAP) Actuators as Artificial Muscles Reality, Potential, and Challenges*. (Y. Bar-Cohen, Ed.) (2nd ed.). Washington: Spie Press.

Bar-Cohen, Y. (2005). Current and future developments in artificial muscles using electroactive polymers. *Expert Review of Medical Devices*, *6*, 731–740.

Bar-Cohen, Y., Kim, K. J., Choi, H. R., & Madden, J. D. W. (2007). Electroactive polymer materials. *Smart Materials and Structures*, *16*.

Bele, A., Cazacu, M., Stiubianu, G., & Vlad, S. (2014). Silicone-barium titanate composites with increased electromechanical sensitivity. the effects of the filler morphology. *Royal Society of Chemistry Advances*, *4*, 58522.

Bele, A., Cazacu, M., Stiubianu, G., Vlad, S., & Ignat, M. (2015). Polydimethylsiloxane-barium titanate composites: Preparation and evaluation of the morphology, moisture, thermal, mechanical and dielectric behavior. *Composites Part B: Engineering*, *68*, 237–345.

Bele, A., Stiubianu, G., Varganici, C. D., Ignat, M., & Cazacu, M. (2015). Silicone dielectric elastomers based on radical crosslinked high molecular weight polydimethylsiloxane co-filled with silica and barium titanate. *Journal of Materials Science*, *50*, 6822–6832.

Beşergil, B. (2003). *Polimer Kimyası*. Ankara: Gazi Kitabevi.

Bistričič, L., Borjanovič, V., Zamboni, I., Jakšič, M., & McGuire, G. E. (2014). Spectroscopic study of poly(dimethylsiloxane) ZnO nanocomposites exposed to proton irradiation. *Macromolecular Symposia*, *339*, 91–99.

Cakmak, E. (2014). *Dielectric and electromechanical properties of polyurethane and polydimethylsiloxane blends and nanocomposites*, Phd Thesis, North Carolina State University, North Carolina.

Callister, W. D., & Rethwisch, D. G. (2014). *Materials science and Engineering An Introduction* (9th ed.). USA: Wiley.

Carter, C. B., & Norton, M. G. (2007). *Ceramic Materials: Science and Engineering*. New York: Springer.

Chen, L., Lu, L., Wu, D., & Chen, G. (2007). Silicone rubber/graphite nanosheet electrically conducting nanocomposite with a low percolation threshold. *Polymer Composites*.

Cheng, Z. Y., Bharti, V., Xu, T. B., Xu, H., Mai, T., & Zhang, Q. M. (2001). Electrostrictive poly(vinylidene fluoride-trifluoroethylene) copolymers. *Sensors*

and Actuators, A: Physical, *90*, 138–147.

Cho, W.-S., & Hamada, E. (1998). Synthesis of ultrafine $BaTiO_3$ particles from polymeric precursor: their structure and surface property. *Journal of Alloys and Compounds*, *266*, 118–122.

Choi, W., Choi, K., Yang, G., Kim, J. C., & Yu, C. (2016). Improving piezoelectric performance of lead-free polymer composites with high aspect ratio $BaTiO_3$ nanowires. *Polymer Testing*, *53*, 143–148.

Clark, I. J., Takeuchi, T., Ohtori, N., & Sinclair, D. C. (1999). Hydrothermal synthesis and characterisation of $BaTiO_3$ fine powders: Precursors, polymorphism and properties. *Journal of Materials Chemistry*, *9*, 83–91.

Corning, D. (2013). *Product Information Dow Corning® 184 silicone elastomer*. Retrieved July 20, 2018 from www.dowcorning.com

Dascalu, C., & Maugin, G. A. (1995). On the dynamic fracture of piezoelectric materials. *Quarterly Journal of Mechanics and Applied Mathematics*, *48*(2), 237–255.

de Andrade, M. C., Carneiro, G. N., Moreira, E. L., Araújo, J. C., & Moraes, V. C. A. (2014). Synthesis and Characterization of Barium Titanate by Solid-State Reaction. *Materials Science Forum*, *802*, 285–290.

Eduok, U., Faye, O., & Szpunar, J. (2017). Recent developments and applications of protective silicone coatings: A review of PDMS functional materials. *Progress in Organic Coatings*, *111*, 124–163.

Eguchi, M. (1925). On the Permanent Electret. *Philosophical Magazine*, *49*, 178.

Finkenstadt, V., & Willett, J. L. (2005). Preparation and characterization of

electroactive biopolymers. In *Macromolecular Symposia*.

FRITSCH. (n.d.). *Barium Titanate grinding report*. Retrieved August 12, 2018 from https://www.fritsch-international.com/sample-preparation/grinding-reports/report-details/?no_cache=1&protokoll=19890

Godfrey, J. T. (2017). *Soft Robotic Actuators*. MSc Thesis. University of California, Irvine.

Groza, A., & Surmeian, A. (2015). Characterization of the oxides present in a polydimethylsiloxane layer obtained by polymerisation of its liquid precursor in corona discharge. *Journal of Nanomaterials*.

Hakuta, Y., Ura, H., Hayashi, H., & Arai, K. (2005). Continuous production of BaTiO3 nanoparticles by hydrothermal synthesis. *Industrial and Engineering Chemistry Research*, *44*, 840–846.

Hu, W. (2015). *Synthesizing New Dielectric Elastomers for Actuation*. Phd Thesis. University of California, Los Angeles.

Hu, Y., Lan, T., Wu, G., Zhu, Z., & Chen, W. (2014). A spongy graphene based bimorph actuator with ultra-large displacement towards biomimetic application. *Nanoscale*, *6*, 12703.

Jiang, K., Wang, J., Li, Q., Liu, L., Liu, C., & Fan, S. (2011). Superaligned carbon nanotube arrays, films, and yarns: A road to applications. *Advanced Materials*, *23*, 1154–1161.

Kiss, K., Magder, J., Vukasovich, M. S., & Lockhart, R. J. (1966). Ferroelectrics of Ultrafine Particle Size: I, Synthesis of Titanate Powders of Ultrafine Particle Size. *Journal of the American Ceramic Society*, *49*(6), 291–295.

Kobayashi, Y., Nishikata, A., Tanase, T., & Konno, M. (2004). Size Effect on Crystal Structures of Barium Titanate Nanoparticles Prepared by a Sol-Gel Method. *Journal of Sol-Gel Science and Technology*, *29*, 49–55.

Kornbluh, R. D., Pelrine, R., Joseph, J., Heydt, R., Pei, Q., & Chiba, S. (1999). High-field electrostriction of elastomeric polymer dielectrics for actuation. In *SPIE Conference on Electroactive Polymer Actuators and Devices* (149–161). California.

Lai, W. (2015). *Characterization, fabrication, and analysis of soft dielectric elastomer actuators capable of complex 3D deformation*. Phd Thesis, Iowa State University, Iowa.

Lee, J., Kim, J., Kim, H., Bae, Y. M., Lee, K. H., & Cho, H. J. (2013). Effect of thermal treatment on the chemical resistance of polydimethylsiloxane for microfluidic devices. *Journal of Micromechanics and Microengineering*, *23*, 035007.

Lee, S. W., & Lee, S. S. (2008). Shrinkage ratio of PDMS and its alignment method for the wafer level process. *Microsystem Technologies*, *14*, 205–208.

Li, S., Wu, J., Wang, Z. M., & Jiang Yadong. (2013). Nanoscale Sensors. In S. Li, J. Wu, Z. M. Wang, & Jiang Yadong (Eds.), *Nanoscale Science and Technology 19* (281). Switzerland: Springer.

Liu, C.-X., & Choi, J.-W. (2012). Improved Dispersion of Carbon Nanotubes in Polymers at High Concentrations. *Nanomaterials*, *2*, 329–347.

Madden, J. D. W., Vandesteeg, N. A., Anquetil, P. A., Madden, P. G. A., Takshi, A., Pytel, R. Z., … Hunter, I. W. (2003). Artificial muscle technology: Physical principles and naval prospects. *IEEE Journal of Oceanic Engineering*, 19.

Madsen, M. H., Feidenhans'l, N. A., Hansen, P. E., Garnæs, J., & Dirscherl, K. (2014). Accounting for PDMS shrinkage when replicating structures. *Journal of Micromechanics and Microengineering*, 10.

Maison, W., Kleeberg, R., Heimann, R. B., & Phanichphant, S. (2003). Phase content, tetragonality, and crystallite size of nanoscaled barium titanate synthesized by the catecholate process: effect of calcination temperature. *Journal of the European Ceramic Society*, *23*, 127–132. Retrieved July 25, 2018 from www.elsevier.com/locate/jeurceramsoc

Malghe, Y. S., Gurjar, A. V., & Dharwadkar, S. R. (2004). Synthesis of BaTiO3 powder from barium titanyl oxalate (BTO) precursor employing microwave heating technique. *Bulletin of Materials Science*, *27*(3), 217–220.

Martinček, I., Turek, I., & Tarjányi, N. (2014). Effect of boundary on refractive index of PDMS. *Optical Materials Express*, *4*(10), 9.

Mata, A., Fleischman, A. J., & Roy, S. (2005). Characterization of polydimethylsiloxane (PDMS) properties for biomedical micro/nanosystems. *Biomedical Microdevices*, *7*(4), 281–293.

McCrum, N. G., Buckley, C. P., & Bucknall, C. B. (1997). *Principles of polymer engineering* (2nd ed.). Oxford: OXFORD University Press.

McDonald, J. C., & Whitesides, G. M. (2002). Poly(dimethylsiloxane) as a material for fabricating microfluidic devices. *Accounts of Chemical Research*, *35*(7), 491–499.

Moghtada, A., & Ashiri, R. (2016). Enhancing the formation of tetragonal phase in perovskite nanocrystals using an ultrasound assisted wet chemical method. *Ultrasonics Sonochemistry*, *33*, 141–149.

Moraes, C., Sun, Y., & Simmons, C. A. (2009). Solving the shrinkage-induced PDMS alignment registration issue in multilayer soft lithography. *Journal of Micromechanics and Microengineering*, *19*, 065015.

Nayak, S., Chaki, T. K., & Khastgir, D. (2013). Development of Poly(dimethylsiloxane)/BaTiO 3 Nanocomposites as Dielectric Material. *Advanced Materials Research*, *622–623*, 897–900.

Nayak, S., Chaki, T. K., & Khastgir, D. (2014). Development of Flexible Piezoelectric Poly(dimethylsiloxane)− BaTiO3 Nanocomposites for Electrical Energy Harvesting. *ACS Publication*, *53*, 14982–14992.

Niu, X. (2013). *Dielectric Actuation of Polymers*. Phd Thesis, University of California, Los Angeles.

Özen, M., Mertens, M., Schroeven, M., Snijkers, F., & Cool, P. (2012). Preparation of barium titanate powders and colloidal processing in a strong (9.4 T) magnetic field. *Materials Letters*, *67*, 154–157.

Ozsecen, Y. (2010). *Dielectric electroactive polymer based biomedical devices: control, sensing and interfacing*. MSc Thesis, Northeastern University, Massachusetts.

Pelrine, R., Kornbluh, R., Pei, Q., & Joseph, J. (2000). High-Speed Electrically Actuated Elastomers with Strain Greater Than 100%. *SCIENCE*, *287*, 836–839.

Pietroiusti, A., Stockmann-Juvala, H., Lucaroni, F., & Savolainen, K. (2018). Nanomaterial exposure, toxicity, and impact on human health. *Wiley Interdisciplinary Reviews: Nanomedicine and Nanobiotechnology*, *10*(5), 1–21.

Reed, J. S. (2008). *Principles of Ceramic Processing* (2nd ed.). USA: Wiley.

Ren, K. (2007). *Approaches to Achieve Smarter Electroactive Materials and Devices*. Phd Thesis, The Pennsylvania State University, Pennsylvania.

Ribeiro, C. M. de O. (2012). *Processing and characterization of piezoelectric polymers for tissue engineering applications*. Phd Thesis, Universidade do Minho, Portuguese.

Richerson, D. W., & Lee, W. E. (2018). *Modern Ceramic Engineering Properties, Processing, and Use in Design* (4th ed.). New York: CRC Press Taylor&Francis Group.

Roentgen, W. C. (1880). About the changes in shape and volume of dielectrics caused by electricity. *Annual Physics Ans Chemistry Series*, *11*, 771–786.

Saçak, M. (2012). *Polimer Teknolojisi*. Ankara: Gazi Kitabevi.

Sarıtaş, S., Türker, M., & Durlu, N. (Eds.). (2007). *Toz metalurjisi ve parçacıklı malzeme işlemleri: işlemleri, malzemeler, ürünler, özellikler ve uygulamalar* (5). Ankara: Türk Toz Metalurjisi Derneği.

Schmid, H., & Michel, B. (2000). Siloxane polymers for high-resolution, high-accuracy soft lithography. *Macromolecules*, *33*, 3042–3049.

Shankar, R., Ghosh, T. K., & Spontak, R. J. (2007). Dielectric elastomers as next-generation polymeric actuators. *Soft Matter*, *3*, 1116–1129.

Shankar, R., Ghosh, T. K., & Spontak, R. J. (2009). Mechanical and actuation behavior of electroactive nanostructured polymers. *Sensors and Actuators, A: Physical*, *151*, 46–52.

Trolier-Mckinstry, S. (2008). Crystal chemistry of piezoelectric materials. In A. Safari

& E. K. Akdoğan (Eds.), *Piezoelectric and Acoustic Materials for Transducer Applications* (39–56). Springer Science+Business Media, LLC.

Wu, H., Odom, T. W., Chiu, D. T., & Whitesides, G. M. (2003). Fabrication of complex three-dimensional microchannel systems in PDMS. *Journal of the American Chemical Society*, *125*, 554–559.

Xia, C.-T., Shi, E.-W., Zhong, W.-Z., & Guo, J.-K. (1995). Preparation of BaTiO3, by the Hydrothermal Method. *Journal of the European Ceramic Society*, *15*, 1171–1176.

Xie, S.-H., Zhu, B.-K., Wei, X.-Z., Xu, Z.-K., & Xu, Y.-Y. (2005). Polyimide/BaTiO3 composites with controllable dielectric properties. *Composites: Part A*, *36*, 1152–1157.

Yilgör, E., & Yilgör, I. (2014). Silicone containing copolymers: Synthesis, properties and applications. *Progress in Polymer Science*, *39*, 1165–1195.

Zhoul, J., Li, L., Gui, Z., Zhang, X., & Barber, D. J. (1997). Sol-gel derived BaTiO3 thin films with embedded silver nanoparticles: preparation and dielectric properties. *Nanostructured Materials*, *8*(3), 321–328.

Zhu, X. (2009). Piezoelectric ceramic materials: Processing, properties, characterization, and applications. In W. G. Nelson (Ed.), *Piezoelectric Materials: Structure, Properties...* (36). Nova Science Publishers, Inc. Retrieved August 16, 2018 from https://www.researchgate.net/publication/281563548